

ScholarWorks@GSU

Biophysical Heme Binding Studies of *Corynebacterium diphtheriae* and *Streptococcus pyogenes*

Authors	Thompson, Stephanie
Citation	Thompson, Stephanie. "Biophysical Heme Binding Studies of <i>Corynebacterium diphtheriae</i> and <i>Streptococcus pyogenes</i> ." Thesis, Georgia State University, 2017. https://doi.org/10.57709/10492697
DOI	https://doi.org/10.57709/10492697
Download date	2026-06-09 18:29:06
Link to Item	https://hdl.handle.net/20.500.14694/2914

BIOPHYSICAL HEME BINDING STUDIES OF *CORYNEBACTERIUM DIPHTHERIAE*
AND *STREPTOCOCCUS PYOGENES*

by

STEPHANIE SOPHIA THOMPSON

Under the Direction of Dabney K. W. Dixon, PhD

ABSTRACT

Gram-positive pathogenic bacteria utilize cell-surface anchored proteins to bind and transport heme into the cell. These bacteria acquire iron from host proteins containing heme e.g., hemoglobin. Proteins like HmuT from *Corynebacterium diphtheriae* bind and help transport heme into the cell. Residues His136 and Tyr235 are utilized as the axial ligands, with a conserved Arg237 residue acting as the hydrogen bonding partner to the axial Tyr235. Similarly, *Streptococcus pyogenes* utilizes the cell anchored protein Shr to transfer heme into the cell. Shr-NEAT2 is hexacoordinated by two axial methionines and is prone to autoreduction where lysines are the most likely source of electrons. Lastly, PefR of Group A *Streptococcus* is a DNA transcription factor which regulates protein expression. Preliminary studies indicate a cysteine may coordinate the heme. A combination of UV-visible, resonance Raman, and magnetic circular dichroism spectroscopies shows these proteins play a crucial role heme transport and regulation.

INDEX WORDS: Gram-positive bacteria, Heme, NEAT domains, Autoreduction,

Corynebacterium diphtheriae, *Streptococcus pyogenes*, DNA transcription regulator

BIOPHYSICAL HEME BINDING STUDIES OF *CORYNEBACTERIUM DIPHTHERIAE*
AND *STREPTOCOCCUS PYOGENES*

by

STEPHANIE SOPHIA THOMPSON

A Thesis Submitted in Partial Fulfillment of the Requirements for the Degree of

Master of Science

in the College of Arts and Sciences

Georgia State University

2017

Copyright by
Stephanie Sophia Thompson
2017

BIOPHYSICAL HEME BINDING STUDIES OF *CORYNEBACTERIUM DIPHTHERIAE*
AND *STREPTOCOCCUS PYOGENES*

by

STEPHANIE SOPHIA THOMPSON

Committee Chair: Dabney Dixon

Committee: Donald Hamelberg

Giovanni Gadda

Electronic Version Approved:

Office of Graduate Studies

College of Arts and Sciences

Georgia State University

August 2017

DEDICATION

This thesis is dedicated to my family especially my parents Solomon and Joyce Thompson for their love and support.

ACKNOWLEDGEMENTS

I would like to acknowledge my committee members Dr. Donald Hamelberg and Dr. Giovanni Gadda, for their academic mentorship. To the Gadda group; Elias, Chris, Dan, Archana, Daniel, and Jacob, thank you for always being there to help me troubleshoot my experiments! To my lab mates past and present Dr. Draganova, Dr. Uluisik, Brandon Ferrell, Cyrienne Keutcha, Carly Wieting, thank you for your continued support and friendship over the years. Lastly, to Dr. Dabney Dixon. I have come this far largely credited to your mentorship. Thank you for taking me under your wing. I will carry each one of you with me.

TABLE OF CONTENTS

ACKNOWLEDGEMENTS	V
LIST OF TABLES	X
LIST OF FIGURES	XI
1 CHAPTER 1: INRODUCTION TO HEME UPTAKE IN BACTERIA.....	1
1.1 Heme and Bacterial Virulence	1
1.2 Heme Uptake in Gram-positive Bacteria	2
2 CHAPTER 2: HYDROGEN BONDING PARTNER HMUT R237A OF	
<i>CORYNEBACTERIUM DIPHTHERIAE</i>	3
2.1 Heme Uptake in <i>Corynebacterium diphtheriae</i>.....	3
2.2 Proposed Hydrogen Bonding Partners in Heme Uptake Pathways	5
2.2.1 Tyrosine as a Hydrogen Bonding Partner	5
2.2.2 Arginine as a Hydrogen Bonding Partner	6
2.2.3 Histidine as a Hydrogen Bonding Partner.....	6
2.2.4 Lysine as a Hydrogen Bonding Partner.....	6
2.3 Axial Tyrosine Hydrogen Bonding Partner in Heme Transport Proteins.....	7
2.4 Materials and Methods	8
2.4.1 DNA Extraction WT <i>HmuT</i>.....	8
2.4.2 <i>HmuT</i> R237 Mutation.....	9
2.4.3 Agarose Gel	11

2.4.4	<i>DpnI Digestion</i>	11
2.4.5	<i>Agar Plate Preparation</i>	12
2.4.6	<i>Calcium Chloride Solution Preparation</i>	12
2.4.7	<i>Cell Transformation</i>	12
2.4.8	<i>HmuT R237A Protein Expression</i>	13
2.4.9	<i>HmuT R237A Protein Purification</i>	14
2.5	Results and Discussion	14
3	CHAPTER 3: THE SECOND NEAT DOMAIN SHR IN <i>STREPTOCOCCUS</i>	
	<i>PYOGENES</i>	20
3.1	<i>Streptococcus pyogenes</i> and Heme Uptake	20
3.2	NEAT Domains.....	21
3.3	Autoreduction of Iron Shr-N2.....	22
3.4	Low Spin State Ligands	24
3.5	The Long-Wavelength Charge-Transfer Fe-S Band.....	24
3.6	Axial Methionine Fluxionality	25
	3.6.1 <i>Spectra Mono/Bis Methionine</i>	25
3.7	Materials and Methods	27
	3.7.1 <i>DNA Extraction WT Shr-N2</i>	27
	3.7.2 <i>Shr-N2 K29A and K57A Mutations</i>	27
	3.7.3 <i>Agarose Gel</i>	28

3.7.4	<i>Dpn1 Digestion</i>	29
3.7.5	<i>Transformation</i>	29
3.7.6	<i>Shr-N2 Protein Expression</i>	30
3.7.7	<i>Shr-N2 Protein Purification</i>	30
3.7.8	<i>pH Titration- autoxidation and autoreduction of WT Shr-N2</i>	31
3.7.9	<i>pH Titration- autoxidation and autoreduction of WT Shr-N2</i>	32
3.8	Results and Discussion	32
3.8.1	<i>pH Dependent Autoxidation of WT Shr-N2</i>	33
3.8.2	<i>pH Dependent Autoreduction of WT Shr-N2</i>	39
4	CHAPTER 3: THE DNA TRANSCRIPTION REGULATOR PEFR IN	
	<i>STREPTOCOCCUS PYOGENES</i>	42
4.1	Multiple antibiotic resistance regulators and porphyrin-regulated efflux via PefR	42
4.2	Materials and Methods	43
4.2.1	<i>WT PefR Protein Transformation</i>	43
4.2.2	<i>WT PefR Protein Expression</i>	44
4.2.3	<i>WT PefR Protein Purification</i>	44
4.2.4	<i>Bradford Assay WT PefR</i>	45
4.2.5	<i>Heme Titration of WT PefR</i>	45
4.3	Results and Discussion	46

4.4	General Conclusions	56
	REFERENCES.....	57

LIST OF TABLES

Table 2.1 Selected heme-binding proteins with corresponding residues which are arginine hydrogen-bonded to the axial tyrosine ligand.....	8
Table 2.2 Experimental Primer Data HmuT R237A	9
Table 2.3 Reaction mixtures for PCR of HmuT R237A.....	10
Table 2.4 Polymerase Chain Reaction (PCR) Conditions of HmuT R237A	11
Table 3.1 Charge transfer bands of bis-methionine proteins	25
Table 3.2 Experimental Primer Design for Shr-N2 K29A	27
Table 3.3 Experimental Primer Design for Shr-N2 K57A	27
Table 3.4 Touchdown Polymerase Chain Reaction Conditions for K29A and K57A	28
Table 3.5 Autoxidation rate constants of WT Shr-N2	34
Table 4.1 Purification techniques of DNA bound proteins.....	48
Table 4.2 Comparison of Bach1 to other heme proteins. Taken from ⁸⁴	53

LIST OF FIGURES

Figure 1.1 Structure of heme b.	1
Figure 2.1 Heme uptake system in <i>Corynebacterium diphtheriae</i>	4
Figure 2.2 I-TASSER model of WT HmuT from <i>C. diphtheriae</i> with conserved residues indicated (His136 and Tyr235) and potential hydrogen bonding partners Arg237 and Tyr272.	5
Figure 2.3 UV-visible imaged agarose gel of PCR reactions for HmuT R237A. From left: lanes 1, 2, 3 and 4 correspond to reactions 1, 2, 3 and 4, respectively, from Table 2.3.	15
Figure 2.4 Chromatogram of Strep-Tag R237A shows the isolated protein.	15
Figure 2.5 Overlay of the UV-visible absorption spectra of HmuT WT and mutant R237A, both in 50 mM Tris-Cl buffer at pH 7.0. The spectra were normalized to 1.0 at the Soret. The insert shows the magnified α,β region.	16
Figure 2.6 Thermal folding of WT HmuT. Measuring fraction folded as a function of temperature (°C). WT (blue filled triangle), H136A (green filled square), Y235A (red open diamond), R237A (cyan open square), Y272A (orange filled circle), M292A (magenta open triangle), Y349A (purple open circle), and Y349F (grey filled diamond). Samples were in 50 mM potassium phosphate, pH 7.0 Taken from ³⁸	17
Figure 2.7 Backbonding correlation plot of $\nu\text{Fe-CO}$ versus $\nu\text{C-O}$ for ferrous carbonyls of heme proteins As-isolated WT (blue), H136A (green), and Y235A (red) are shown as open stars while M292A (magenta), and R237A (cyan) are shown as solid stars on the plot. Catalase, blue hexagon [60]; HasA, open circle; CCP, open square; HRP, filled triangle; P450, open triangle; globins, filled square; p22HBP, open diamond; HO-1(H25Y), blue upside down triangle and BSA, blue sideways tri- angle. The dashed grey line is the least-	

squares line for six-coordinate Fe–CO adducts in which the proximal ligand is thiolate or imidazolate; the dotted grey line is the least-squares line for Fe–CO adducts with proximal His (neutral imidazole). The solid blue line represents tyrosine-ligated heme proteins with the guanidinium group of Arg available for hydrogen bonding to the Tyr and the dashed blue line which the ligand trans to CO is coordinated through a neutral oxygen atom. Taken from ³⁸	19
Figure 3.1 Heme uptake system in <i>Streptococcus pyogenes</i>	21
Figure 3.2 Crystal structure of IsdX2 NEAT-5 domain from <i>Bacillus anthracis</i>	22
Figure 3.3 Proposed autoreduction scheme of Shr-N2.	23
Figure 3.4 Homology model of Shr-N2 showing axial ligands M26 and M136; potential electron donors K29 and K57.	24
Figure 3.5 MCD of Shr-N2. Performed by Dan Collins and John Dawson	26
Figure 3.6 UV- visible imaged agarose gel of PCR reactions Shr-N2 K29A, K57A, respectively.	32
Figure 3.7 Overlay of Shr-NEAT2 WT and mutants as-isolated.....	33
Figure 3.8 Timescale of ST Shr-N2. Data fit at 410 nm.....	35
Figure 3.9 Timescale of ST Shr-N2. Data fit at 428 nm.....	35
Figure 3.10 Timescale of ST Shr-N2. Data fit at 532 nm.....	36
Figure 3.11 Timescale of ST Shr-N2. Data fit at 560 nm.....	36
Figure 3.12 YC_VI_7. Absorbance vs. wavelength over 24 h for a solution of WT ShrN2 in 20 mM CAPS, MES, and Tris-Cl at pH 6.6. The pH of the sample was adjusted from 10.4 to 6.6 using 1 M HCl. The absorbance at 428 nm decreases while that at 410 nm increases. The α,β bands decrease. Data recorded by Yu Cao.	37

Figure 3.13 Autoxidation of WT Shr-N2 pH 6.1. Sample prepared in TE buffer (10 mM Tris-Cl, 1 mM EDTA pH 8.0). 1 M HCl added to take pH down to 6.1. Spectra followed every 10 min for 24 h. Arrows indicate the increasing and decreasing peaks over time.	38
Figure 3.14 Difference spectra for autoxidation of WT Shr-N2 at pH 6.1.....	38
Figure 3.15 . Absorbance vs. wavelength over 18 h for a solution of WT ShrN2 in 20 mM CAPS, MES, and Tris-Cl at pH 10.4. The pH of the sample was adjusted to 10.4 using 1 M NaOH. The absorbance at 428 nm increases while that at 406 nm decreases. The α,β bands decrease. Data recorded by Yu Cao.....	39
Figure 3.16 Autoreduction of WT Shr-N2 at pH 10.5. Sample prepared in TE buffer (10 mM Tris-Cl, 1 mM EDTA pH 8.0). To the sample, 1 M NaOH was added to take pH up to 10.5. Spectra followed every minute for 2 h then every 10 min for 22 h.	40
Figure 3.17 Difference spectra for autoreduction of WT Shr-N2 at pH 10.5.....	41
Figure 4.1 Construct of PefR	46
Figure 4.2 Sequence alignment of PefR showing proper transformation of plasmid in cell line.	47
Figure 4.3 SDS gel of WT PefR elution. Lane 1. Protein Ladder. Lane 2. Mixed Ladder [BSA (66.5 kD), myoglobin (16.7 kD)]. Lane 3-7. Fractions containing PefR.....	49
Figure 4.4 I-TASSER model of PefR showing potential axial ligands	49
Figure 4.5 UV-visible absorption spectra of WT PefR.....	50
Figure 4.6 Heme Titration of PefR. Protein (5 μ M) was prepared in 100 mM Tris-Cl, 150 mM NaCl pH 8.0. Hemin in DMSO (1 μ L of an 807 μ M stock) added every 15 min to both the solution of PefR and a blank containing buffer only. Spectra are shown as a function of the concentration of hemin.	51
Figure 4.7 Absorbance at 390 nm as a function of the ratio of hemin to PefR.....	52

Figure 4.8 Ratio of the 390 nm to 280 nm bands as a function of the ratio of hemin to PefR	52
Figure 4.9 UV-visible absorption spectra of WT PefR. The blue spectrum is his-tagged PefR. The red spectrum is strep-tagged PefR.	54
Figure 4.10 WT HrtR in the apo form with DNA (left PDB 3VOK) and holo form (right PDB 3VP5) ⁸⁷	55
Figure 4.11 Crystal structure of <i>S. aureus</i> MepR bound to DNA 72. Highlighted in blue is residue I106, which corresponds to C106 in PefR, the putative heme axial ligand.	55

1 CHAPTER 1: INTRODUCTION TO HEME UPTAKE IN BACTERIA

1.1 Heme and Bacterial Virulence

Iron is a micronutrient necessary for the survival of many pathogenic organisms and is required for bacterial virulence¹⁻³. Although abundant in nature, free iron is often inaccessible in biological systems. Bacterial species have developed different systems to take up heme in iron-depleted environments. One mechanism involves direct contact between the bacterium and the iron sources. Another mechanism is dependent on the synthesis of molecules, referred to as siderophores and/or hemophores, to be secreted by the bacterium to sequester iron from exogenous sources⁴.

The most abundant iron sources in biological systems are found in the form of heme. Heme is a cofactor with an iron atom in the center of a protoporphyrin ring. Protoporphyrin rings are composed of four pyrrole rings linked together by a variation of methine (=CH-) bridges, methyl groups, vinyl groups, and propionic acid side chains. The iron atom in the center of the ring can be found in the ferric (Fe^{3+}) or ferrous (Fe^{2+}) state. There are four major types of biologically relevant hemes: heme A, heme B, heme C, and heme O. Heme B, the most common, is iron protoporphyrin itself (Figure 1.1).

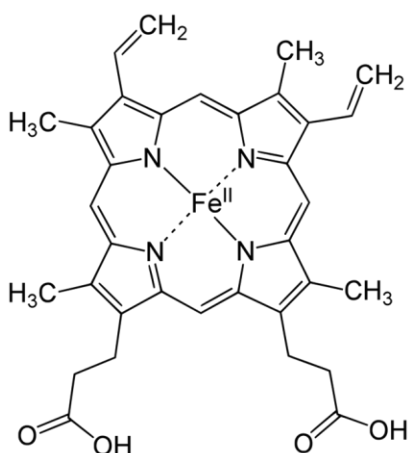


Figure 1.1 Structure of heme b.

Structurally, heme A contains a methyl side chain at position eight of the protoporphyrin ring oxidized to a formyl group and an isoprenoid chain group attached to one of the vinyl side chains. Heme C differs by two covalent thioester linkages to the apoprotein through the vinyl groups. Heme O has a methyl group at position eight instead of a formyl group. Heme is found in proteins such as hemoglobin, the oxygen-transport metalloprotein in red blood cells⁵⁻⁷.

Bacterial virulence often determines the pathogenicity of an organism. Pathogens are becoming increasingly more resistant to commonly used antibiotics⁸. Bacterial cells, which have developed resistance, continue to multiply, resulting in a resistant population that is then transmitted from person to person. Bacteria use different biochemical mechanisms to counter antibiotic pressure: antibiotic-degrading enzymes, antibiotic-altering enzymes, and antibiotic efflux pumps. Alternatively, eliminating the nutritional sources of these pathogens, such as iron in the form of heme, could be effective in deterring the growth of these bacteria. Therefore, heme uptake studies in pathogenic bacteria may allow development of an alternative approach to combat antibiotic resistance.

1.2 Heme Uptake in Gram-positive Bacteria

The heme uptake systems of gram-positive bacteria have been described in *Bacillus anthracis*⁹, *Staphylococcus aureus*^{10, 11}, *Streptococcus pyogenes*^{12, 13}, and *Corynebacterium* species^{14, 15}. Gram-positive bacteria possess a thick cell wall formed by a peptidoglycan layer; composed of glycopolymers, teichoic acids, and carbohydrates¹⁶. Anchored to the cell wall are proteins which shuttle heme from an extracellular source into the cell via ATP-binding cassette (ABC) transporters. ABC transporter proteins are highly conserved membrane proteins that use energy derived from the hydrolysis of ATP to drive transport of compounds across the lipid

bilayer¹⁷. ABC transporters can be classified into either importers or exporters. Importers catalyze the uptake of molecules. They have low substrate affinity and therefore associate with the periplasmic bound proteins that serve as primary binding sites due to their high affinity for substrates. Exporters get rid of toxic materials and waste products. They recruit their substrates directly¹⁷. Heme binds to either the surface of these proteins or is scavenged by hemophores. The heme is then transferred along a protein pathway to reach the intracellular environment. Once inside the cell, heme oxygenase catalyzes the degradation of the heme moiety resulting in the release of the iron^{18,19}. The focus of this thesis will be on the mechanistic features of specific heme uptake proteins from the bacterial pathogens *Corynebacterium diphtheriae* and *S. pyogenes*.

2 CHAPTER 2: HYDROGEN BONDING PARTNER HMUT R237A OF *CORYNEBACTERIUM DIPHTHERIAE*

2.1 Heme Uptake in *Corynebacterium diphtheriae*

Corynebacterium diphtheriae is a gram-positive bacterial pathogen, the causative organism of diphtheria, a severe upper respiratory tract infection in humans¹⁴. Diphtheria is widespread in third world countries lacking resources for proper vaccination²⁰. The ability of pathogenic bacteria such as *C. diphtheriae* to obtain iron during infection is essential for virulence²¹. To date, pathogenic bacterial heme uptake pathways that have been characterized in detail involve ATP-binding cassette (ABC) transporters, shown in Figure 2.1.

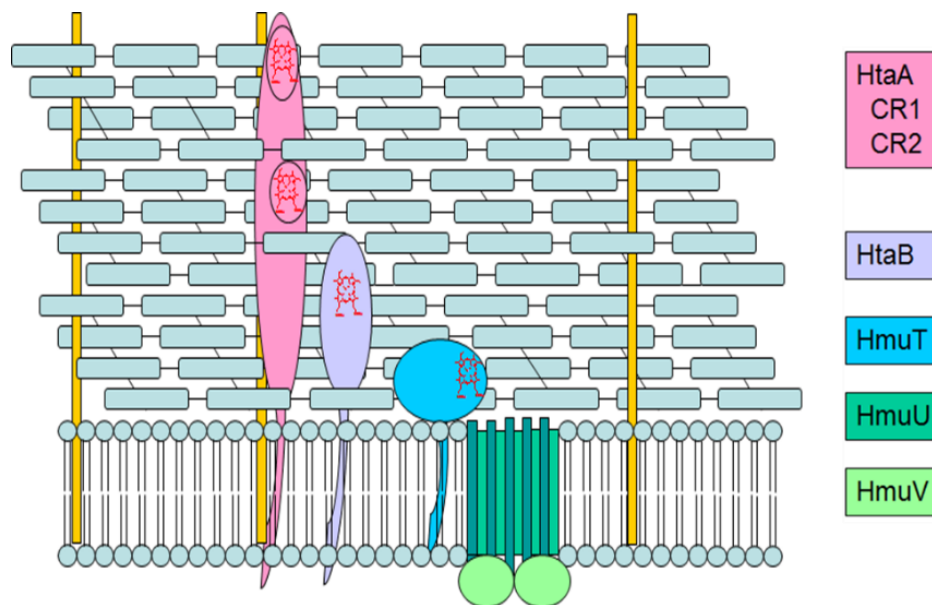


Figure 2.1 Heme uptake system in *Corynebacterium diphtheriae*.

Three genes *hmuT*, *hmuU*, and *hmuV* in *C. diphtheriae* code for one of the ABC-type heme transporters responsible for transporting heme into the cell¹⁴. HmuU and HmuV are the permease and ATPase components, respectively. HmuT has been shown to be a hemin binding lipoprotein anchored to the cytoplasmic membrane by an N-terminal lipid moiety and is responsible for transporting heme to the ABC transporter HmuUV. Homology modeling, UV-visible spectroscopy, resonance Raman spectroscopy, and magnetic circular dichroism suggested that the conserved His136 and Tyr235 residues serve as the heme axial ligands (Figure 2.2)²².

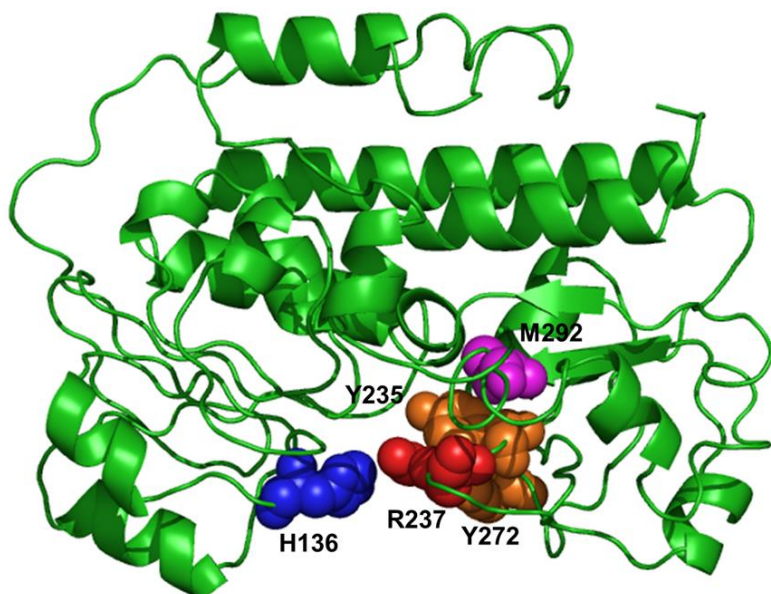


Figure 2.2 I-TASSER model of WT HmuT from *C. diphtheriae* with conserved residues indicated (His136 and Tyr235) and potential hydrogen bonding partners Arg237 and Tyr272.

2.2 Proposed Hydrogen Bonding Partners in Heme Uptake Pathways

The factors that cause heme uptake and release are of significance in understanding heme transfer in pathogenic bacteria. One possibility for control of this process involves changes in the hydrogen bonding to the heme or its axial ligands. The sections below review aspects of literature studies on hydrogen bonding to residues involved in heme binding in the pocket of various heme proteins.

2.2.1 Tyrosine as a Hydrogen Bonding Partner

Bacillus anthracis is a gram-positive bacterium that is the causative agent of anthrax. *B. anthracis* secretes a hemophore, IsdX1, to acquire heme from host hemoglobin and enhance bacterial replication in iron-starved environments²³. IsdX1 then transports the bound heme to the surface protein IsdC where it is carried into the cell. The crystal structure of IsdX1 revealed

the heme is by the axial ligand residue Tyr136, which forms a hydrogen bond with the phenolate oxygen of Tyr140, with a distance of 2.3 Å.

2.2.2 Arginine as a Hydrogen Bonding Partner

Pseudomonas aeruginosa utilizes the periplasmic binding protein PhuT, required to shuttle heme from the outer membrane to the inner membrane of the cell²⁴. The heme of PhuT is embedded in a cleft between the N- and C-terminal domains and is coordinated by Tyr71 from the C-terminus, as the heme ligand²⁴. An arginine in the proximal pocket (Arg73) hydrogen-bonds to the axial tyrosinate ligand. The distance between the bonding sites of the two residues is 4.3 Å, somewhat long for a classical hydrogen bond.

2.2.3 Histidine as a Hydrogen Bonding Partner

Serratia marcescens is a gram-negative bacterium and is responsible for many hospital-acquired infections in the United States²⁵⁻²⁷. This pathogen obtains the iron from hemoglobin through the secretion of the hemophore HasA^{28, 29}. HasA takes up the heme from hemoglobin and shuttles it to the receptor HasR, which in turn, releases heme into the bacterium³⁰. The axial ligands were determined to be His32 and Tyr75³⁰. The phenolate group of Tyr75 has an YxxxxxxxH motif and is thought to be involved in a hydrogen bond with His83. The distance between those two residues is 2.7 Å.

2.2.4 Lysine as a Hydrogen Bonding Partner

Shigella dysenteriae is a gram-negative bacterium that resides in the human gastrointestinal tract. This pathogen causes an inflammatory disorder of the lower digestive tract in humans. *S. dysenteriae* encodes a periplasmic binding protein, ShuT, required to shuttle heme from the outer membrane to the inner membrane^{31, 32}. The heme-ShuT complex contains a five-coordinate high-spin heme that is linked to the protein through a proximal Fe³⁺-O bond to the

phenolate side chain of Tyr67³². It is also proposed that Tyr228 of ShuT may make a significant contribution to the stability of heme-loaded ShuT, without directly interacting with the heme iron³². The crystal structure showed the axial Tyr67 reorients itself when heme is introduced. Tyr67 can point “in” toward the heme pocket, in the position to coordinate the heme iron, or flip out to the surface³². For the partially holo crystals, Tyr67 points inward; in the apo crystal, Tyr67 is shown to point outward. Thus there is considerable flexibility in the orientation of Tyr67. The change in conformation of the axial ligand may contribute to hydrogen-bonding to Lys69³².

2.3 Axial Tyrosine Hydrogen Bonding Partner in Heme Transport Proteins

The majority of proteins in heme transport pathways studied to date utilize tyrosine as an axial ligand^{1, 3, 9, 16, 33-35}. The axial tyrosine is thought to be found in the tyrosinate form, which in turn, keeps the heme iron in the Fe³⁺ state, resulting in a low reduction potential due to this favored interaction³⁶⁻³⁸. Most tyrosine-ligated hemes have an additional residue near the pocket which hydrogen bonds to the heme. Altering hydrogen bonding to these axial tyrosines may play a role in triggering heme uptake and release. This interaction cannot be directly observed in crystal structures of proteins. Many of these interactions are predicted based on homology modeling or sequence alignment analyses. Mutations of these predicted hydrogen bonding partners have served in many instances to show that the predicted interactions are indeed key in proper stabilization of the bound heme. For *C. diphtheriae* HmuT, it is proposed that Arg237 hydrogen bonds to the axial tyrosine, Tyr235. The examples in literature of arginine residues that hydrogen bond to the axial tyrosine are shown in Table 2.1.

Table 2.1 Selected heme-binding proteins with corresponding residues which are arginine hydrogen-bonded to the axial tyrosine ligand.

Protein	Axial Ligation	Residue Hydrogen Bonding Axial Tyrosine	Motif ^a	Arg ⁺ -N ^ω to O-Tyr (Å)	Arg ⁺ -N ^δ to O-Tyr (Å)	PDB	Reference
<i>Y. pestis</i> HmuT	Y70/H167	R72	YxR	2.8	3.8	3NU1	³⁹
<i>C. glutamicum</i> HmuT	H141/Y240	R242	YxR	2.9	2.7	5AZ3	⁴⁰
<i>C. diphtheriae</i> HmuT	H136/Y235	R273 ⁱ	YxR	3.0	2.9	-	⁴¹
<i>C. diphtheriae</i> HmuT H136A	Y235	R273 ⁱ	YxR	2.9	3.0	-	⁴¹
<i>P. homomalla</i> cAOS	Y353	R349	RxxxY	2.8	2.9	1U5U	⁴²
Bovine liver catalase	Y357	R353	RxxxY	2.8	3.4	8CAT	⁴³
<i>M. avium</i> ssp. <i>paratuberculosis</i> MAP	Y294	R290	RxxxY	2.7	2.7	3E4Y	⁴⁴

¹ Residues that represent hydrogen bonding via homology modeling and spectroscopic studies

In *Y. pestis* and *C. diphtheriae*, HmuT hydrogen-bonds with an YxR motif; alternatively, for the other bacteria models, tyrosine hydrogen bonds to arginine by utilizing an RxxxY motif.

2.4 Materials and Methods

2.4.1 DNA Extraction WT HmuT

The HmuT clone was a gift of Dr. Michael Schmitt. DNA extraction was performed using the QIAprep Spin Miniprep Kit (50) from the company QIAGEN. A bacterial overnight culture (5 mL) was pelleted by centrifugation at 10,000 rpm for 3 min at 15 °C. The bacterial pellet was resuspended in 250 μL of Buffer P1 (50mM Tris-Cl, pH 8.0, 10mM EDTA, 100ug/mL RNase A) and transferred to a microcentrifuge tube. Buffer P2 (200mM NaOH, 1% SDS), 250 μL, was

added and mixed thoroughly. Buffer N3 (neutralization buffer) (350 μ L) was immediately added to the mixture. It was centrifuged for 15 min at 155,556 g at 15 °C. The supernatant was applied to a QIAprep spin column. The column was washed with 750 μ L of Buffer PE (wash buffer) and transferred to a collection tube. The solution was centrifuged for 2 min at 155,556 g at 15 °C. The flow-through was discarded and the spin column was placed in a clean microcentrifuge tube. To elute the DNA, 50 μ L of Buffer EB (10mM Tris-Cl, pH 8.5) was added to the spin column, and was centrifuged for 1 min at 155,556 g at 15 °C.

2.4.2 *HmuT R237 Mutation*

Residue Arg237 was mutated to Ala237 via primers shown in Table 2.2.

Table 2.2 Experimental Primer Data HmuT R237A

Oligo Name	MW	T_m °C	Dimer	Secondary Structure	GC%	DNA Sequence
HmuT R237A Forward	9340	80.2	No	Moderate	53.3	GCATTTTTGTATGCGG CGGGTAACGGTGGT
HmuT R237A Reverse	9074	80.2	No	Moderate	53.3	ACCACCGTTACCCGCC GCATACAAAATGC

Multiple reactions conditions were prepared and run on the PCR Eppendorf Mastercycler Gradient. The reactions are shown in Table 2.3.

Table 2.3 Reaction mixtures for PCR of HmuT R237A

Reaction mixture	1	2	3	4
Plasmid (140 ng)	1 μ L	1 μ L	1 μ L	1 μ L
Forward Primer [Rxn 1,2 (540 ng)] [Rxn 3,4 (1000 ng)]	6 μ L	6 μ L	12 μ L	12 μ L
Reverse Primer [Rxn 1,2 (540 ng)] [Rxn 3,4 (1000 ng)]	6 μ L	6 μ L	12 μ L	12 μ L
dNTPmix (100 mM)	1 μ L	1 μ L	1 μ L	1 μ L
DMSO [Rxn 1,3 (2%)] [Rxn 2,4 (1%)]	2.5 μ L	1 μ L	2.5 μ L	1 μ L
10x Pfu Reaction Buffer	5 μ L	5 μ L	5 μ L	5 μ L
Nanopure water	27.5 μ L	29 μ L	15.5 μ L	17 μ L
Pfu polymerase (2.5 U/ μ L) Agilent	1 μ L	1 μ L	1 μ L	1 μ L
Total reaction volume	50 μ L	50 μ L	50 μ L	50 μ L

PCR was performed on the listed reactions using the “hot start” method. This included 18 cycles of melting, annealing and extending (Table 2.4). After cycles were completed, the reactions were held at 4 °C overnight.

Table 2.4 Polymerase Chain Reaction (PCR) Conditions of HmuT R237A

Cycle	Temperature	Time	Number of Cycles
Hot Start	95 °C	2 min	1
Melting	95 °C	30 sec	18
Annealing	72 °C	1 min	
Extension	68 °C	10 min	
Final Extension	68 °C	10 min	1
Hold	4 °C	overnight	1

2.4.3 Agarose Gel

A gel was run to ensure proper formation of desired plasmid. A 1% (w/v) agarose powder (0.5 g), nanopure water (49 mL), and TAE 50 x buffer (1 mL) were added to a Pyrex bottle. To form the gel, the mixture was placed in a water bath and boiled until fully dissolved. The solution was cooled (~ 5 min) and the contents were poured into gel cast to solidify. The samples containing each reaction were arranged. The PCR samples (10 μ L) were mixed with DNA 6x loading dye (2 μ L) from Thermo Fisher Scientific. The solidified gel was immersed in a running buffer containing, nanopure water (980 mL) and TAE 50x buffer (20 mL). Each sample was loaded into an individual well (12 μ L) and run at 70 V for 70 min. The gel was imaged using the Benchtop 3UV Transilluminator Imaging System.

2.4.4 DpnI Digestion

Reaction 3 (see Table 2.3) was digested using FastDigest DpnI from Thermo Fisher Scientific. A solution containing reaction 3 (38 μ L), DpnI buffer (5 μ L), nanopure water (6 μ L) and DpnI (1 μ L) was prepared. The solution was held at 37 °C for 1 h using the PCR Eppendorf

Mastercycler gradient instrument. An additional microliter of DpnI enzyme was added to ensure the digestion of all methylated DNA. The reaction mixture was held at 37 °C for an additional hour. The sample was stored overnight at 20 °C.

2.4.5 Agar Plate Preparation

Agar plates were prepared (4) to proceed with transformation of plasmid to competent cells. Luria-Bertani (LB) medium (2 x 50 mL) containing tryptone (0.5 g), sodium chloride (0.5 g), yeast extract (0.25 g), and agarose (0.75 g) was prepared. The medium was autoclaved (20 min cycle). Both solutions were left to slightly cool (~ 5 min) and 25 µL of a 100 mg/mL stock solution of kanamycin was added (final 50 µg/mL) to one medium for the transformation step. In sterile environment, the contents of each flask were poured into two plates and left to solidify. The plates were then stored in refrigerator (4 °C).

2.4.6 Calcium Chloride Solution Preparation

A 100 mM calcium chloride solution was prepared (100 mL). A solution containing 75 mM calcium chloride dihydrate (1.1 g), 15% glycerol (15 mL), 10 mM PIPES (0.3 g), and 5 mM magnesium chloride hexahydrate (0.1 g) was added to a beaker. Nanopure water was added (90 mL) and the pH was adjusted to 7.0 using 3 M sodium hydroxide. Nanopure water was used to adjust the volume to 100 mL.

2.4.7 Cell Transformation

An *E. coli* BL21 cell line was used in this experiment to later express the protein. The cells were grown overnight in LB media (10 mL). The cells grown overnight (2 mL), were left to grow in a large scale medium (100 mL) at 225 rpm and 37 °C. The flask was placed on ice once an OD of 0.6 was reached. The contents of the flask were equally fractioned out into two falcon tubes and spun at 4,580 rpm for 10 min at 4 °C. The supernatant was discarded and

calcium chloride solution (20 mL) was added. The pellet was resuspended and then left to sit for 10 min. The solution was spun at 4,580 rpm for 10 min at 4 °C. The supernatant was drained and calcium chloride (4 mL) was added. The digested PCR reaction 3 solution (1 µL) and now competent cells (50 µL) was incubated in a microcentrifuge tube on ice for 20 min. The solution was heat shocked in a water bath at 4 °C for 45 sec, then immediately placed back on ice for 2 min. The solution (51 µL) was then added to warm LB media (250 µL) and shook at 37 °C for 1 h. The sample was streaked on two agar plates with kanamycin and left to grow overnight at 37 °C. One colony was chosen and half was grown in LB media (10 mL) for DNA extraction. The other half of the same colony was used to streak a new agar plate with kanamycin.

2.4.8 HmuT R237A Protein Expression

LB media was prepared by adding 10 g of tryptone, 10 g of sodium chloride, 5 g of yeast extract and 1,000 mL of Barnstead Diamond Nanopure water into four 2 L flasks. All media was sterilized for a 20 min cycle, using a Steris Amsco Renaissance autoclave. After cooling for 3-4 h to room temperature, 500 µL of 100 mM kanamycin was added to each 2 L flask. To separate 125 mL flasks, 25 mL of the broth containing kanamycin was added and inoculated with a R237A glycerol stock solution, using the sterile flame loop technique. All flasks were incubated in a New Brunswick Scientific Excella E24 incubator shaker, at 37 °C on 220 rpm for approximately 16 h. The contents were then returned to the 2 L flasks containing the remaining LB and kanamycin, to allow for growth on a larger scale. Using a Varian 50 Bio UV-visible spectrophotometer, the optical density (OD) readings at 600 nm were taken as a function of time. Once the absorbance reached an OD₆₀₀ between 0.6 and 0.8 (approximately 3 h), the media was induced with 1 mL of 100 mM isopropyl β-D-1-thiogalactopyranoside (IPTG). The temperature was reduced to 27 °C and the media continued shaking for another 3 h. The cells were harvested

using a JLA 8.100 in a rotor Beckman Coulter Avanti-T26 XPI centrifuge at 8,000 g for 30 min at 4 °C. The cell pellets were stored at 80 °C.

2.4.9 *HmuT R237A Protein Purification*

The R237A cell pellets were placed in a beaker, on ice, containing 174 mL buffer A (100 mM Tris-Cl, 150 mM NaCl, pH 8.0), 20 mL of 100 mM magnesium chloride, 2 mL of 10 mM phenylmethylsulfonyl fluoride (PMSF), 4.0 mL of 10 mg/mL lysozyme, and 5 µg/mL each of DNase I Recombinant (Lot 14636800) and RNase A (Lot 70297724) (Roche Diagnostics) from bovine pancreas. After the mixture had been homogenized, the sample was lysed on ice for 20 min using a Fisher Scientific Sonic Dismembrator Model 500 Sonicator. The settings of the experiment was 20 sec pulse on time and 5 sec pulse off time with an amplitude of 15%. Once lysed, the samples were centrifuged using an Eppendorf Centrifuge 5804R 15 amp Version at 6,500 rpm at 4 °C for 30 min. The supernatant was collected and the pellets discarded.

The following purification steps were conducted at 4 °C using a GE Healthcare ÄKTA fast protein liquid chromatography (FPLC, Amersham BioSciences); all buffer solutions were adjusted to pH 8.0. The sample (~ 50 mL) was loaded onto a Strep-Tactin Superflow column (5 mL, IBA BioTAGnology) equilibrated with buffer A (100 mM Tris-HCl, 150 mM NaCl, pH 8.0). Unbound material was washed out with 5 column volumes (CV) of buffer A. The mutant was eluted with 10 CV of buffer B containing 100 mM Tris-HCl, 150 mM NaCl, 2.5 mM desthiobiotin applied via a linear gradient.

2.5 Results and Discussion

The results from the agarose gel of reaction three produced the desired product (Figure 2.3). After expressing R237A, it was purified. The chromatogram shows that pure protein was

obtained (Figure 2.4). This sample further was run on SDS gel and pure fractions were collected and stored. In the batch of protein expressed, 3.2 mg/mL (5 mL) was obtained.

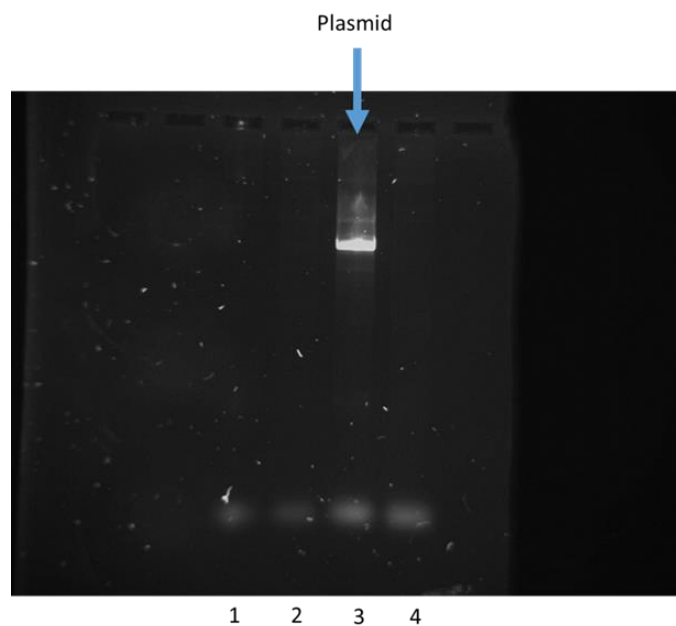


Figure 2.3 UV-visible imaged agarose gel of PCR reactions for HmuT R237A. From left: lanes 1, 2, 3 and 4 correspond to reactions 1, 2, 3 and 4, respectively, from Table 2.3.

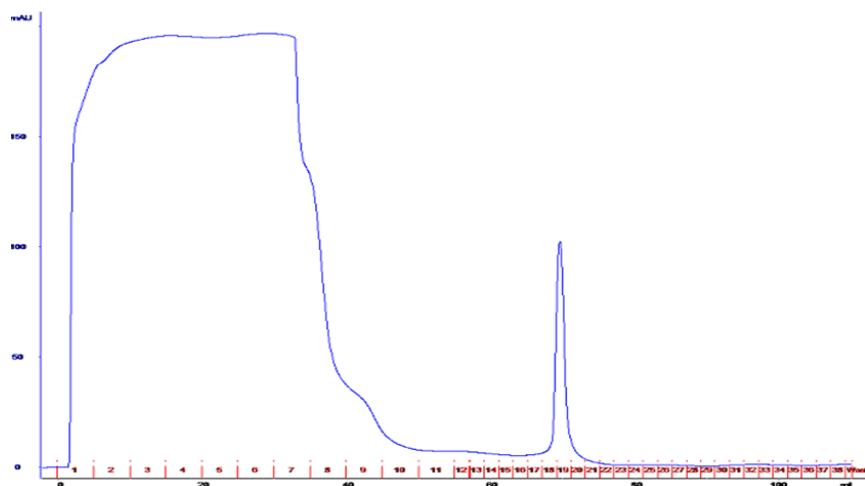


Figure 2.4 Chromatogram of Strep-Tag R237A shows the isolated protein.

In general, to calculate heme binding, the extinction coefficient of the heme in a heme protein is used ($1 \times 10^5 \text{ M}^{-1} \text{ cm}^{-1}$ at the Soret). The ratio of the absorbance of the Soret: 280 can give a rough estimate of the heme loading of the protein. As isolated, WT *CdHmuT* is ~80% heme loaded, whereas the as-isolated R237A mutant is only ~40% heme loaded. The reduction in heme loading of the mutant in comparison to the WT protein may indicate that Arg237 plays a role in maintaining heme integrity. Figure 2.5 shows an overlay of the two UV-visible absorption spectra, normalized to 1.0 at the Soret (~400 nm).

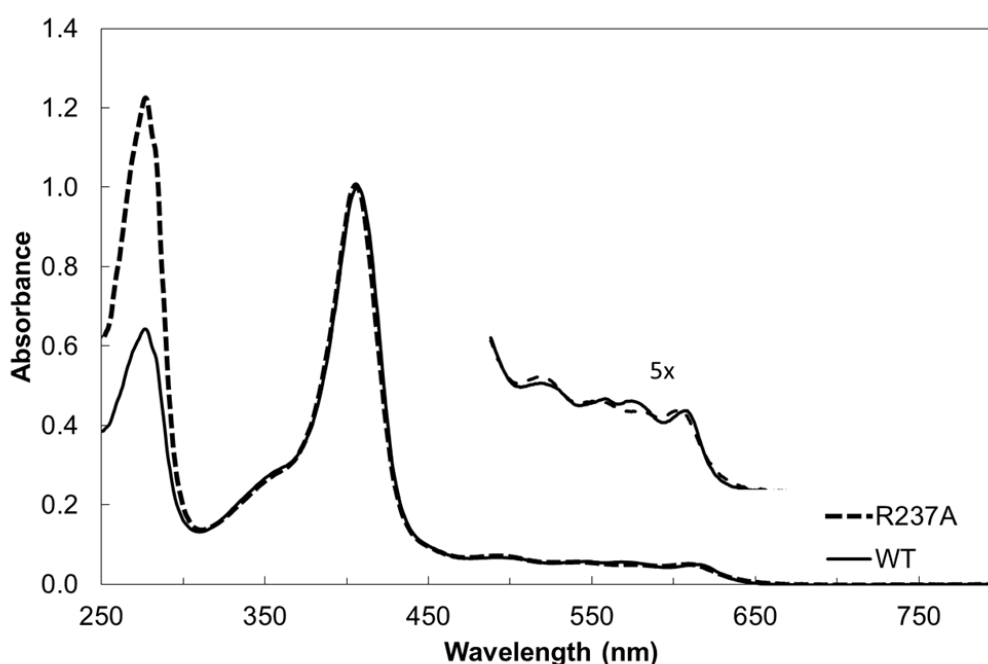


Figure 2.5 Overlay of the UV-visible absorption spectra of *HmuT* WT and mutant R237A, both in 50 mM Tris-Cl buffer at pH 7.0. The spectra were normalized to 1.0 at the Soret. The insert shows the magnified α, β region.

There is very little spectral difference between the WT and R237A, indicating that Arg237 may be in or near the heme pocket, but is not directly interacting with the heme. This is consistent with the *C. glutamicum* structure of *HmuT* which shows that arginine is a hydrogen bonding partner to the axial tyrosine⁴⁵. It would be expected that the UV-visible absorbance

spectrum of R237A would change dramatically if the arginine residue had a direct interaction with the heme. For example, the UV-visible absorption spectra of the HmuT heme with mutated axial ligands (H136A and Y235A) vary in both the position of the Soret band and the number of bands in the α,β -region⁴¹. Although this residue was not directly observed as a heme ligand, Arg237 is conserved across multiple species of *Corynebacterium* and was therefore studied in more detail.

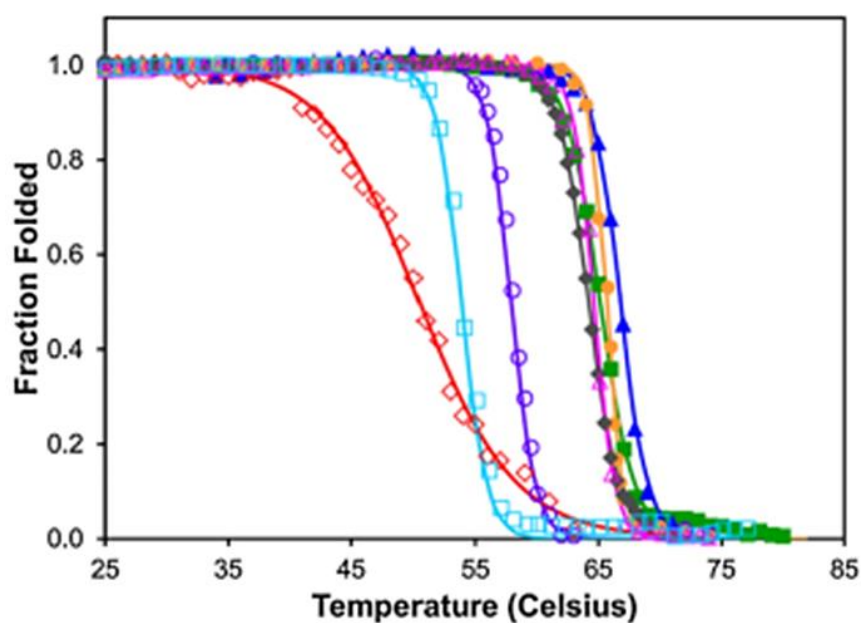


Figure 2.6 Thermal folding of WT HmuT. Measuring fraction folded as a function of temperature (°C). WT (blue filled triangle), H136A (green filled square), Y235A (red open diamond), R237A (cyan open square), Y272A (orange filled circle), M292A (magenta open triangle), Y349A (purple open circle), and Y349F (grey filled diamond). Samples were in 50 mM potassium phosphate, pH 7.0 Taken from⁴¹.

WT HmuT gave a T_m of 66.8 °C while R237A gave a T_m of 54.0 °C. This supports the idea that the axial tyrosine needs Arg237 to maintain the integrity of the heme in the pocket as the T_m of this mutant is reduced by ~13 °C as compared to the WT.

Resonance Raman spectroscopy was also used to help support the argument that Arg237 is the hydrogen bonding partner to the axial tyrosine. A back-bonding correlation, in which the frequency of the Fe-CO bond stretch is plotted against the frequency of the Fe-CO bond stretch for the ferrous carbonyls of HmuT is shown in Figure 2.7⁴¹. Oxygen-based heme ligands appear in the lowest energy quadrant of the graph. With the addition of the HmuT examples to the plot, and particularly with the addition of R237A, it became clear that the classical single linear correlation could be divided into two. Previous studies done on nitric oxide synthase complexes showed that a strong hydrogen-bond donation could weaken the strength of the proximal ligand⁴¹. This led to an investigation of the hydrogen bonding partners of the proteins on the plot. A detailed study of the x-ray structures of known proteins indicated that the upper line involves hydrogen bonding to arginine (two hydrogen bonds), while the lower line involves a single hydrogen bond.

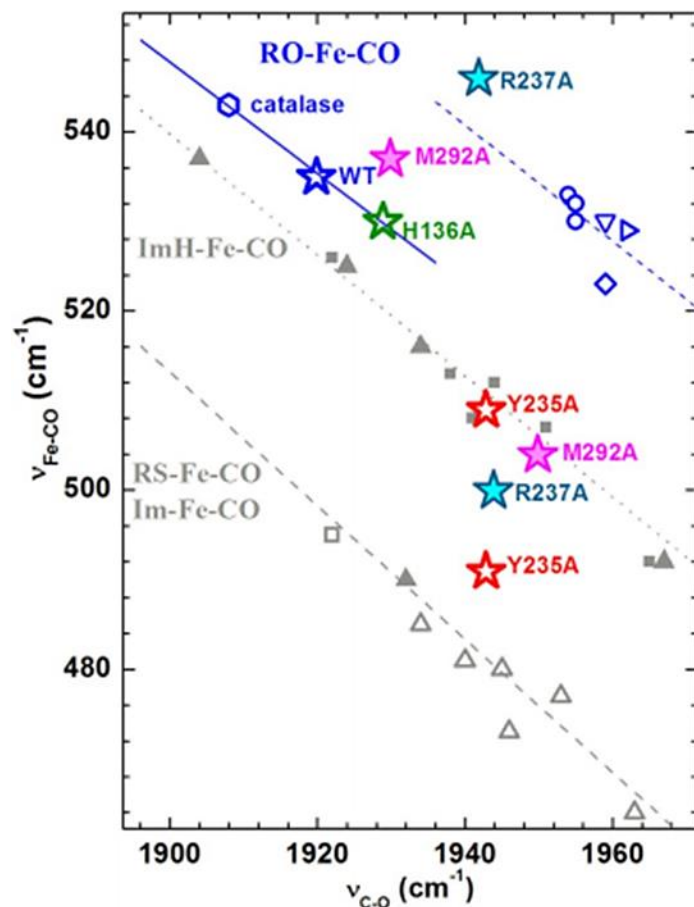


Figure 2.7 Backbonding correlation plot of $\nu_{\text{Fe-CO}}$ versus $\nu_{\text{C-O}}$ for ferrous carbonyls of heme proteins. As-isolated WT (blue), H136A (green), and Y235A (red) are shown as open stars while M292A (magenta), and R237A (cyan) are shown as solid stars on the plot. Catalase, blue hexagon [60]; HasA, open circle; CCP, open square; HRP, filled triangle; P450, open triangle; globins, filled square; p22HBP, open diamond; HO-1(H25Y), blue upside down triangle and BSA, blue sideways triangle. The dashed grey line is the least-squares line for six-coordinate Fe-CO adducts in which the proximal ligand is thiolate or imidazolate; the dotted grey line is the least-squares line for Fe-CO adducts with proximal His (neutral imidazole). The solid blue line represents tyrosine-ligated heme proteins with the guanidinium group of Arg available for hydrogen bonding to the Tyr and the dashed blue line which the ligand trans to CO is coordinated through a neutral oxygen atom. Taken from ⁴¹.

The guanidinium group of arginine, with a bifurcated hydrogen bond, weakens the Fe-CO bond, therefore shifting the correlation line up as shown in Figure 2.7 ⁴¹. There are a handful of crystallized proteins that employ Try-Arg hydrogen-bonding (Table 2.1) ⁴¹, all of which are in

position to have similar distances to the axial tyrosine. The Raman data are in accord with the hypothesis that R237 is in position to be the hydrogen bonding partner to Y235 of HmuT.

Our work has shown that not only the axial ligands of heme proteins are required for heme binding, but also other residues in the pocket. In particular, R237 serves as the hydrogen-bonding partner to the axial Y235. Removal of this residue gives a similar UV-visible absorbance profile, yet the heme binding capacity of the protein is reduced by 50%. Thermal melting studies of this R237A mutant, compared to the WT, showed the overall stability of the protein was reduced upon removal of this residue. The resonance Raman spectra are consistent with serving as a hydrogen bonding partner to Y235. Overall, these studies add to the growing number of identified hydrogen bonding heme protein motifs and reiterate that multiple residues contribute to the ability of efficient heme binding in these proteins.

3 CHAPTER 3: THE SECOND NEAT DOMAIN SHR IN *STREPTOCOCCUS PYOGENES*

3.1 *Streptococcus pyogenes* and Heme Uptake

Streptococcus pyogenes is a gram-positive pathogenic bacterium belonging to group A β -hemolytic streptococcus (GAS) bacteria^{12, 46-48}. β -hemolytic bacteria break down red blood cells. These bacteria are responsible for a wide range of infections and diseases including streptococcal pharyngitis, acute pharyngitis, rheumatic heart disease, impetigo, and cellulitis. GAS obtains required iron need as a nutritional source from heme⁴⁹. Heme sources include hemoglobin, the hemoglobin:haptoglobin complex, heme albumin, myoglobin, and catalase.

Heme is first transferred to the streptococcal hemoprotein receptor (Shr), a large membrane-anchored protein. Shr has a hydrophobic tail that is positively charged associating it

with the cytoplasmic membrane⁴⁹. This cell-surface protein contains two NEAT domains, Shr-NEAT1 (Shr-N1) and Shr-NEAT2 (Shr-N2). Shr-N1 is preceded in the sequence by a distinctive N-terminal domains (NTD); Shr lacks the cell-wall anchoring motif that is found in Isd receptor proteins of *S. aureus*⁴⁹. Shr-N1 obtains heme from the extracellular space and is able to transfer to either Shr-N2 or directly to Shp (streptococcal cell surface protein)⁴⁹. Heme is then transferred to the ABC heme transporter encoded by the *sia* (streptococcal iron acquisition) gene cluster¹², also known as the *hts* (heme transport *S. pyogenes*) gene cluster⁵⁰. And is shuttled into the cell as depicted in Figure 3.1.

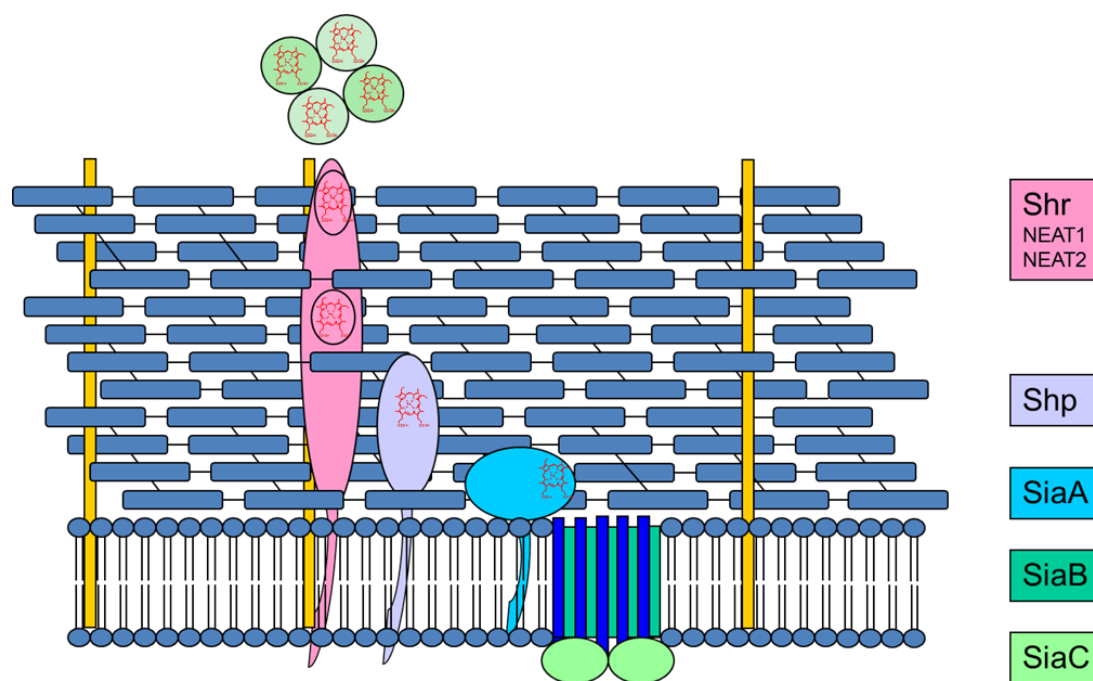


Figure 3.1 Heme uptake system in *Streptococcus pyogenes*.

3.2 NEAT Domains

The *S. pyogenes* heme uptake pathway utilizes two near iron transport (NEAT) domains during heme transfer. NEAT domains consist of conserved secondary structural features including β -strands and a 3_{10} α -helix⁵¹. The classical NEAT heme-binding motif involves an

YXXXY motif in which the first Tyr from the β -8 strand is an axial ligand and the second tyrosine is a hydrogen-bonding partner to the first⁵². An example of a typical NEAT domain structure is shown in Figure 3.2.

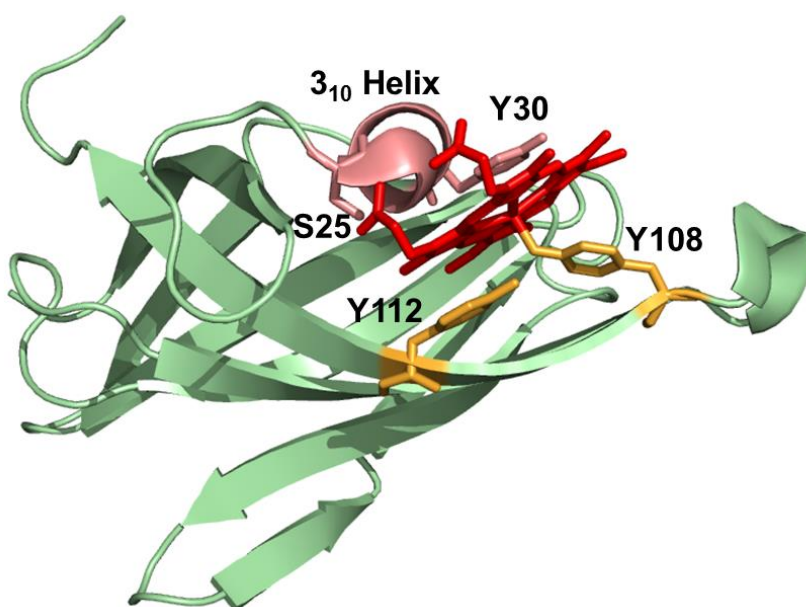


Figure 3.2 Crystal structure of IsdX2 NEAT-5 domain from *Bacillus anthracis*.

In recent years, variations on this theme have been discovered. *S. aureus* IsdB-N2 has a Met/Tyr axial ligand set⁵³. IsdA binds tyrosine in the ferric state and histidine in the ferrous state⁵⁴. *Bacillus anthracis* HalA utilizes a YXXXXF motif, rather than YXXXY⁵⁵. The proposed hemophore Hbp2 (Hbp2-N2) from *Listeria monocytogenes* differs in that the axial tyrosine extends from the β -7 strand, rather than the β -8 strand⁵⁶. This emerging variety among heme axial ligand motifs of NEAT proteins may imply the ability of these proteins to play roles other than binding and transferring heme to the next protein in the pathway.

3.3 Autoreduction of Iron Shr-N2

Shr-N1 is predicted to utilize a bis-methionine axial ligation set to coordinate the heme iron, as indicated by sequence alignment, homology modeling, and various spectroscopic

analyses. Sequence alignment of Shr-N1 with Shr-N2 indicated that Shr-N2 to also uses a bis-methionine axial ligand set with an M26 N-terminal ligand and an M136 C-terminal ligand. Shr-N2 is isolated as a mixture of the Fe(II) and Fe(III) forms of the protein. This is not surprising as heme proteins with methionine ligands typically have higher reduction potentials, making it easier to change oxidation states. Interestingly, Shr-N2 is prone to autoreduction of the heme, unlike the sister domain Shr-N1 which does not autoreduce, although it proposed to have the same axial ligands as Shr-N2. The Shr-N2 heme autoreduces as the pH increases and autoxidizes as the pH decreases; the process occurs in about two hours. The most likely cause of autoreduction could be attributed to nearby lysine residues. A proposed scheme of this process is shown in Figure 3.3. The facile change in oxidation states may be physiologically significant. Figure 3.4 shows the homology model of Shr-N2 and those proposed lysine responsible for autoreduction. Heme transfer studies between Shr-N1 and Shr-N2 was shown to be reversible and may indicate Shr-N2 is used as a storage source of heme⁴⁹. Based on these findings, it could be the case that in environments with high levels of iron, Shr-N2 could store the heme until the iron levels become too low, in which the heme could be passed back to Shr-N1 and re-enter the pathway.

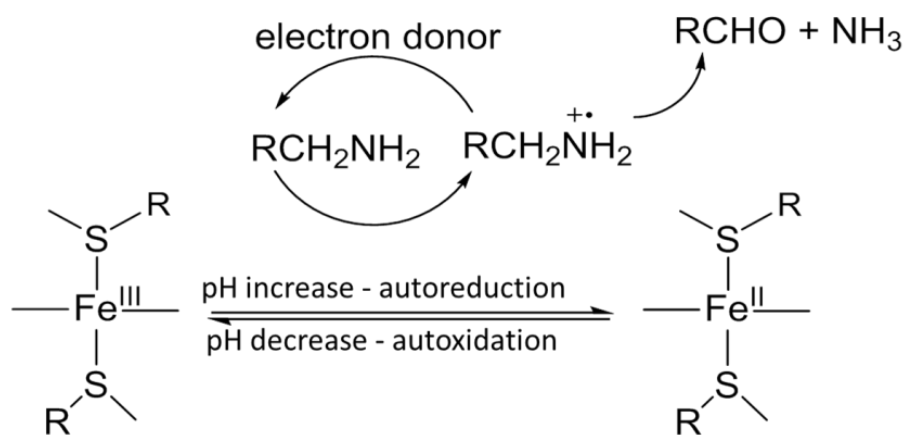


Figure 3.3 Proposed autoreduction scheme of Shr-N2.

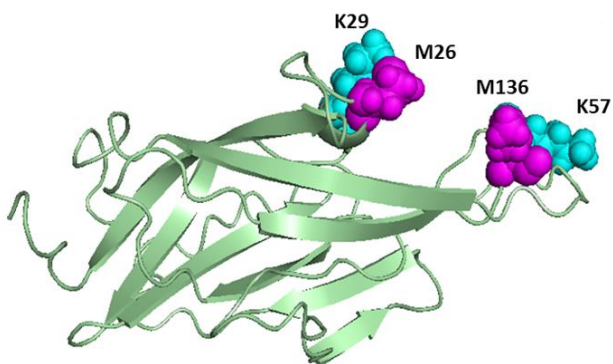


Figure 3.4 Homology model of Shr-N2 showing axial ligands M26 and M136; potential electron donors K29 and K57.

3.4 Low Spin State Ligands

Low-spin state ligands forcibly pair electrons within the $3d$ orbital resulting in the formation of octahedral complexes. Amino acid residues such as histidine, methionine, cysteine and lysine have ligand field strengths which generate this low spin state. These bis-coordinate heme centers often undergo electron transfer reactions due to the redox change at the metal ion. Studies of low-spin cytochromes show bis-histidine and methionine/histidine coordination are the most common ligation combinations. However, lysine/histidine has been observed in mitochondrial cytochrome *c*⁵⁷, and bis-methionine ligation in bacterioferritin⁵⁸⁻⁶¹. Therefore, it could be the case that Shr-N2 K29 and K57 are nearby the proposed heme methionine ligands in order to carry out the electron transfer reactions required for heme storage or other protein functions.

3.5 The Long-Wavelength Charge-Transfer Fe-S Band

It has long been known that the Fe-S bond in heme gives rise to a long wavelength charge transfer band. Perhaps the best-known example is cytochrome *c*, in which the bond occurs at 695 nm. Table 3.1 gives a compilation of known methionine-ligated proteins; charge-transfer

transitions tend to be sensitive to the oxidation state on the central iron. It is observed that the charge transfer band primarily arises when the iron is under an oxidized high-spin state. The approximate wavelengths however, vary greatly between 600 nm – 695 nm.

Table 3.1 Charge transfer bands of bis-methionine proteins

Class	Protein	$\lambda_{\text{nm charge transfer}}$	$\sim \epsilon (\text{M}^{-1} \cdot \text{cm}^{-1})$	Reference
Met/His	Cytochrome <i>c</i>	695	830	⁶²
	IsdE	650	5.00×10^4	⁶³
	SiaA	-	-	⁶⁴
Met/Met	Bacterioferritin	734	1.25×10^3	⁶⁰
	Shp	-	-	⁶⁵
	H102M cytochrome b_{562}	610	7.4×10^{-3}	⁶⁶
	Shr NEAT1	~ 645	-	This work
	Shr NEAT2	~ 640	-	This work
Met/Tyr	IsdB-N2	630	2.0×10^4	⁵³

3.6 Axial Methionine Fluxionality

It is postulated that there is a low intrinsic affinity of thioether for ferric heme ⁶⁷. The most common example would be cytochrome *c* where it is seen that donor ligands have the ability to frequently replace the axial methionine under an oxidative state. The mobility of the iron-thioether bond is proposed to be important to the function of these proteins. This mobility is attributed to conformational changes in heme axial methionine seen by hyperfine shifts in NMR spectra ⁶⁸. It is suggested that the sulfur bond of the methionine side chain becomes inverted. These orientations contribute to the fluxionality of the axial methionine caused by this heme pocket strain.

3.6.1 Spectra Mono/Bis Methionine

Spectroscopic studies of mono and bis-methionine ligation proteins are limited to the few known examples of these systems. With the addition of low concentrations of

tetrahydrothiophene (THT) to exogenous ligand-free ferric H93G Mb, spectral changes were observed consistent with what would be observed for a mono-methionine ligated protein⁶⁹. In particular, a red shift of the Soret maximum and an intensity increase of the charge transfer band at approximately 600 nm were seen⁶⁹. The ligand *trans* to the axial methionine was thought to be a hydroxide group. At high concentrations of THT and at high pH, bis-THT H39G Mb could be observed via MCD. In comparison with the mono-THT, the Soret was more red shifted and the intensity of the α,β bands increased. However, the charge transfer band around 600 nm decreased⁶⁹. Similar studies were performed on Shr-N2 by Dan Collins and John Dawson. The MCD at pH 6.5 of Shr-N2 is similar to that of bis-THT. At pH 10, the MCD is consistent with mono-THT, as shown in Figure 3.5.

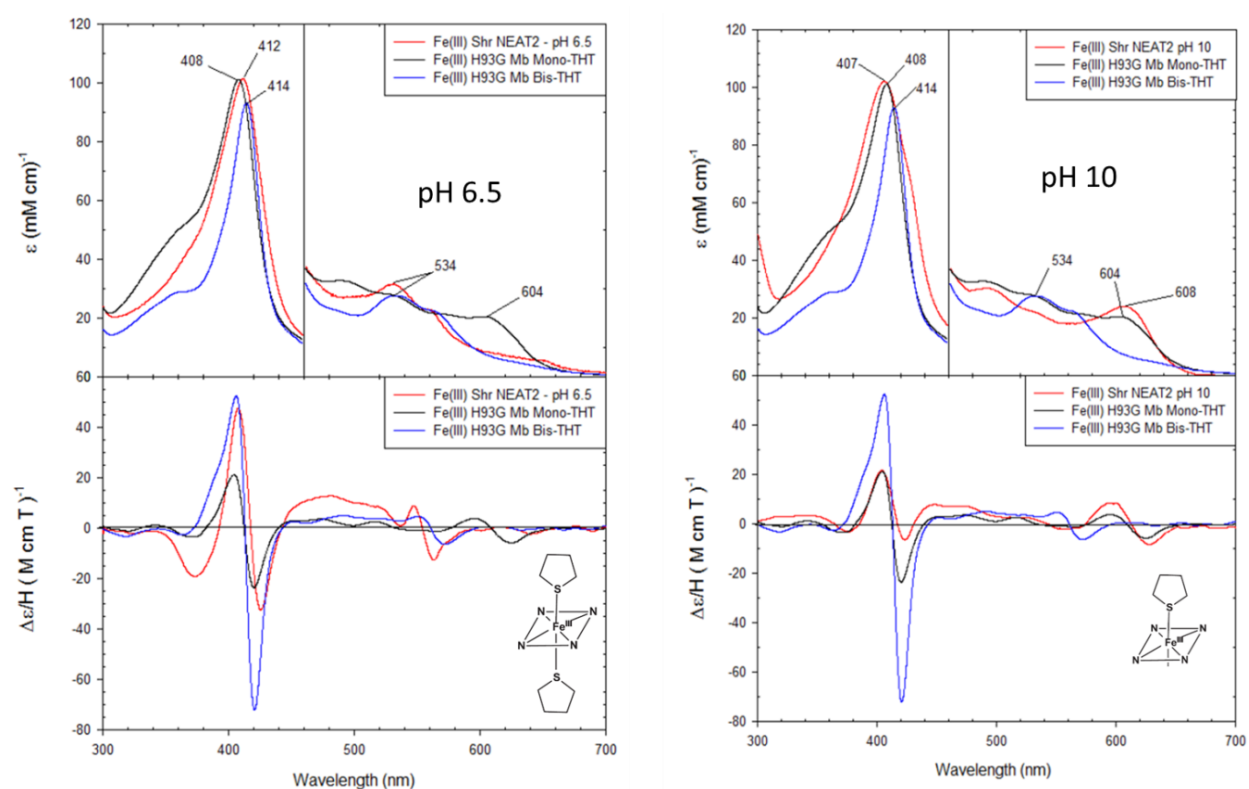


Figure 3.5 MCD of Shr-N2. Performed by Dan Collins and John Dawson

3.7 Materials and Methods

3.7.1 DNA Extraction WT Shr-N2.

DNA extraction was performed using the QIAprep Spin Miniprep Kit (50) from the company QIAGEN. A series of buffers and centrifugation techniques were used to extract the DNA from the plasmid by following the kit manual provided.

3.7.2 Shr-N2 K29A and K57A Mutations

The Shr-N2 WT clone was a gift from Dr. Zehava Eichenbaum. The sequence of Shr-N2 was re-verified. Residues K29 and K57 were mutated to A29 and A57 (Table 3.2-3.3) respectively via PCR reactions shown in Table 3.4.

Table 3.2 Experimental Primer Design for Shr-N2 K29A

Oligo Name	MW	T _m °C	Dimer	Secondary Structure	GC%	DNA Sequence
Shr-N2 K29A Forward	9951	72.6	No	Moderate	46.8	GGTATAAAGGTTGGTGCGATGTTAGGCTACCT
Shr-N2 K29A Reverse	10014	73.0	No	Moderate	45.4	AAGGTAGCCTAACATCGCACCAACCTTTATACC

Table 3.3 Experimental Primer Design for Shr-N2 K57A

Oligo Name	MW	T _m °C	Dimer	Secondary Structure	GC%	DNA Sequence
Shr-N2 K29A Forward	9951	72.6	No	Moderate	46.8	GGTATAAAGGTTGGTGCGATGTTAGGCTACCT
Shr-N2 K29A	10014	73.0	No	Moderate	45.4	AAGGTAGCCTAACATCGCACCAACCTTTATACC

Reverse						
---------	--	--	--	--	--	--

Primer designs were checked in the Sigma Oligo program; this company provided the primers. Multiple reactions conditions were run for PCR. A variation in the DMSO concentration (2% and 5%) and the amount of plasmid used varied in the reactions as shown in Table SP16 F. PCR was performed on the listed reactions using the touchdown method.

Table 3.4 Touchdown Polymerase Chain Reaction Conditions for K29A and K57A

Cycles	Temperature	Time	Number of Cycles
Hot Start	95 °C	2 min	1
Melting	95 °C	30 sec	20
Annealing	63 °C-72 °C	1 min	
Extension	68 °C-72 °C	10 min	
Final Extension	68 °C-72 °C	10 min	1
Hold	4 °C	overnight	1

This included 25 cycles of melting, annealing and extending. After the cycles were completed, the reactions were held at 4 °C overnight.

3.7.3 Agarose Gel

A gel was run to ensure proper formation of desired plasmid. A 1% (w/v) agarose powder (0.5 g), nanopure water (49 mL), and TAE 50 x buffer (1 mL), previously prepared, were added to a Pyrex bottle. To form the gel, the mixture was placed in a water bath and heated until fully dissolved. The solution was cooled (~ 5 min) and the contents were poured into gel cast to solidify. The samples containing each reaction was then prepared. The PCR samples (10 µL

each) were mixed with DNA 6x loading dye (2 μL each). A ladder solution was prepared using nanopure water (4 μL), 6x loading dye (1 μL), and 1 kb DNA Ladder (1 μL) provided by New England BioLabs Inc. The solidified gel was immersed in a running buffer containing, nanopure water (980 mL) and TAE 50x buffer (20 mL). Each sample was loaded into each individual well (12 μL) and run at 70 V for 70 min. The gel was imaged using the Benchtop 3UV Transilluminator Imaging System.

3.7.4 *DpnI* Digestion

Reaction 1 was digested using DpnI. A solution containing reaction 1 (38 μL), DpnI buffer (5 μL), nanopure water (6 μL) and DpnI (1 μL) was prepared. The Thermocycler was used to digest reaction 1. The solution was held at 37 °C for 1 h. Another 1 μL aliquot of DpnI enzyme was added to ensure the digestion of all methylated DNA and was held at 37 °C for an additional hour. The sample was stored overnight at 20 °C.

3.7.5 *Transformation*

E. coli BL21 DE3 (New England BioLabs) cell line was used in this experiment to transform the mutated plasmid. Reaction 3 solution (1 μL) and competent cells (50 μL) was incubated in a microcentrifuge tube on ice for 20 min. The solution was heat shocked in a water bath at 4 °C for 45 sec, then immediately placed back on ice for 2 min. The solution (51 μL) was added to warm LB media (250 μL) and left to shake at 37 °C for 1 h. The sample was streaked on two agar plates with kanamycin and incubated overnight at 37 °C. One colony was chosen and half was grown in LB media (10 mL) for DNA extraction. The other half of the same colony was used to streak a new agar plate. The DNA extracted was sequenced at GENEWIZ.

3.7.6 *Shr-N2 Protein Expression*

LB media was prepared by adding 10 g of tryptone, 10 g of NaCl, 5 g of yeast extract and 1 L of nanopure water from Barnstead Diamond into four 2 L flasks. All media was sterilized for 20 min, using a Steris Amsco Renaissance autoclave. After cooling for 3-4 h to room temperature, 500 μ L of 100 mM kanamycin was added to each 2 L flask. To separate 125 mL flasks, 25 mL of the broth containing kanamycin was extracted and inoculated with the stock solution previously made, using the sterile flame loop technique. All flasks were incubated in a shaker, at 37 °C on 220 revolutions per minute (rpm) for approximately 16 h. The contents were then returned to the 2 L flasks containing the remaining LB and kanamycin, to allow for growth on a larger scale. Optical density readings at 600 nm were taken as a function of time. Once the absorbance reached an OD between 0.5 and 0.7 (approximately 3 h), the media was induced with 1 mL of 100 mM isopropyl β -D-1-thiogalactopyranoside. The temperature was reduced to 27 °C and the media continued shaking for another 3 h. The cells were harvested and centrifuged at 8,000 G for 30 min at 4 °C. The cell pellets were stored in the 1 L centrifuge tubes at 80 °C.

3.7.7 *Shr-N2 Protein Purification*

The Shr-N2 cell pellet was homogenized, on ice, in a solution containing buffer A (100 mM Tris-Cl, 150 mM NaCl, pH 8.0), 100 mM magnesium chloride, 10 mM phenylmethylsulfonyl fluoride, 10 mg/mL lysozyme, 5 μ g/mL each of DNase I Recombinant (Lot 14636800), and RNase A (Lot 70297724) from Roche Diagnostics. The solution was lysed for 30 min (10 sec pulse on time and 10 sec pulse off time, amplitude of 15%). Once lysed, the samples were centrifuged at 7,000 rpm at 4 °C for 45 min. The supernatant was collected and stored.

The following purification steps were conducted at room temperature and all buffer solutions were adjusted to pH 8.0. The sample (40 mL) was loaded onto a Strep-Tactin Superflow column (5 mL, IBA BioTAGnology) equilibrated with buffer A (100 mM Tris-HCl, 150 mM NaCl, pH 8.0). Unbound material was washed out with 5 column volumes (CV) of buffer A. The mutant was eluted with 10 CV of buffer B containing 100 mM Tris-HCl, 150 mM NaCl, 2.5 mM desthiobiotin, pH 8.0 applied via a linear gradient. This sample was stored in the -80 °C freezer. Roughly 2.3 mg/mL was purified from each expression batch.

3.7.8 pH Titration- autoxidation and autoreduction of WT Shr-N2

The spectra of Shr-N2 WT were measured as a function of pH. The first experiments were run previously by Yu Cao. In the first titration experiment, WT Shr-N2 in 20 mM each CAPS, MES, and Tris-Cl was taken to pH 10.5 with 1 M NaOH. This sample was followed by UV-visible spectroscopy every 10 min for the first 2 h and every 30 min for the next 17 h. The pH of this sample was then adjusted to 6.1 using 1 M HCl and UV-visible absorption spectra taken every 10 min for 24 h. The pH was then adjusted to 10.5 using 1 M NaOH and UV-visible absorption spectra were taken every 10 min for 24 h. In the second titration experiment, the buffer was exchanged to 20 mM each CAPS, MES, and Tris-Cl at pH 6.5 and the sample was held at this pH for 2 h until ΔA_{Soret} was less than 0.001 over 10 min. The sample was then taken to pH 10.1 and the spectrum recorded every 10 min for 24 h.

The experiment was rerun on a second batch of protein. The samples were prepared in 20 mM each CAPS, MES, and Tris-Cl. The pH was taken to 6.1 with 1 M HCl; UV-visible absorption spectra were taken every 10 min for 24 h. In the second experiment, the pH of this sample was adjusted to 10.5 using 1 M NaOH and, again, UV-visible absorption spectra were taken every 10 min for 24 h. Rate constants for both trials were determined and compared.

3.7.9 pH Titration- autoxidation and autoreduction of WT Shr-N2

A sample of WT Shr-N2 was prepared in 10 mM Tris-Cl and 1mM EDTA pH 8.0 (TE buffer). Each sample was first adjusted to pH 6.1 using 1 M HCl. The spectra was followed every 10 min for 24 h. The pH was then adjusted to 10.5 and their spectra were followed every min for the first 2 h and every ten minutes for the remaining 22 h. Data were fit to an equation involving two first-order processes using KaleidaGraph fitting program.

$$A = A_0e^{(-kt)}+A_1e^{(-kt)}+b$$

3.8 Results and Discussion

The results were positive for the mutations of Shr-N2. The gel from PCR experiment was imaged using the Benchtop 3UV Transilluminator Imaging System, as shown in Figure 3.7. All lanes showed the desired product, so reaction 1 was used for digestion. GENEWIZ was used to confirm the correct mutations were obtained.

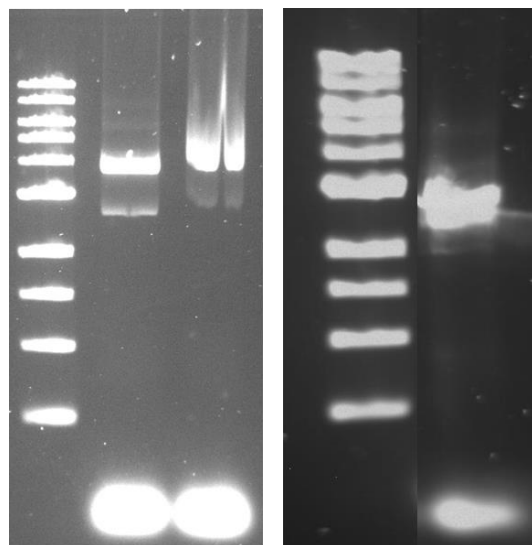


Figure 3.6 UV- visible imaged agarose gel of PCR reactions Shr-N2 K29A, K57A, respectively.

NEAT2 is isolated as a mixture of the oxidized and reduced forms. An overlay of Shr-N2 and the mutants show the differences in spectra as-isolated shown in Figure 3.7. Each batch of protein expressed varies to the percent of reduction after purification as depicted in Figure 3.7.

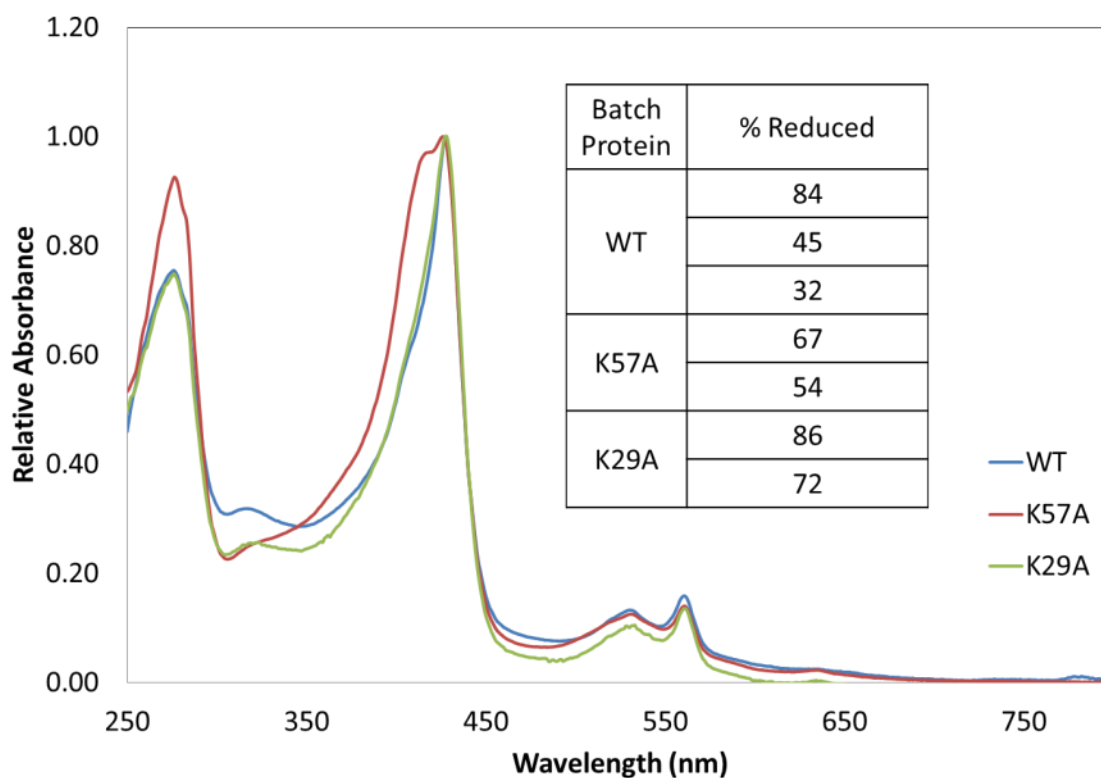


Figure 3.7 Overlay of Shr-NEAT2 WT and mutants as-isolated.

3.8.1 pH Dependent Autoxidation of WT Shr-N2

For experiments run by Yu Cao of WT Shr-N2, a sample was run at pH 6.6, over 24 h. It showed a large variation in the rate constants as a function of pH shown in Figure 3.12. Data at 410 nm were not well-fit by either one or two exponentials (Figures 3.8). The rate constants range from $0.8 - 2 \text{ h}^{-1}$, again about 10 – 20 times that of the second rate constant (Table 3.5).

Table 3.5 Autoxidation rate constants of WT Shr-N2

ST WT pH 6.6					
Abs (nm)	k_1 (h^{-1})	k_2 (h^{-1})	k_1/k_2	% fast phase	% slow phase
410	0.59 ± 0.02	-	-	-	-
428	0.69 ± 0.02	0.09 ± 0.02	7.6	84	16
532	0.57 ± 0.02	-	-	-	-
560	0.68 ± 0.02	0.04 ± 0.01	18.4	65	35
YC WT pH 6.6					
Abs (nm)	k_1 (h^{-1})	k_2 (h^{-1})	k_1/k_2	% fast phase	% slow phase
410	0.41 ± 0.05	-	-	-	-
428	0.79 ± 0.03	0.08 ± 0.01	10.5	16	84
532	2.17 ± 0.49	0.12 ± 0.01	18.1	12	88
560	1.09 ± 0.08	0.09 ± 0.01	12.0	12	88

To compare the reproducibility of the protein, a sample of WT Shr-N2 initially at pH 8 (largely reduced, 88%), 1 M HCl was added to take the solution to pH 6.6. Over 24 h, the Soret peak at 410 nm (oxidized) increased and the peak at 428 nm (reduced) decreased. In the α, β region, both peaks at 532 nm and 560 nm also decrease over time, indicating the oxidation of the protein (Figures 3.13). A rather clean transition is observed, as seen in the difference spectra. Signs of an isosbestic point can be seen at ~ 430 nm (Figure 3.14). Data at 410 and 532 nm were not well-fit by either one or two exponentials (Figures 3.9 and 3.11). Overall, the first process had a rate constant ranging from $0.6 - 0.7 \text{ h}^{-1}$, about 10 – 20 times that of the second rate constant. Comparisons of the autoxidation of both experiments are shown in Table 3.5. Based on the comparison from both experiments, it was concluded that autoxidation of Shr-N2 is irreproducible.

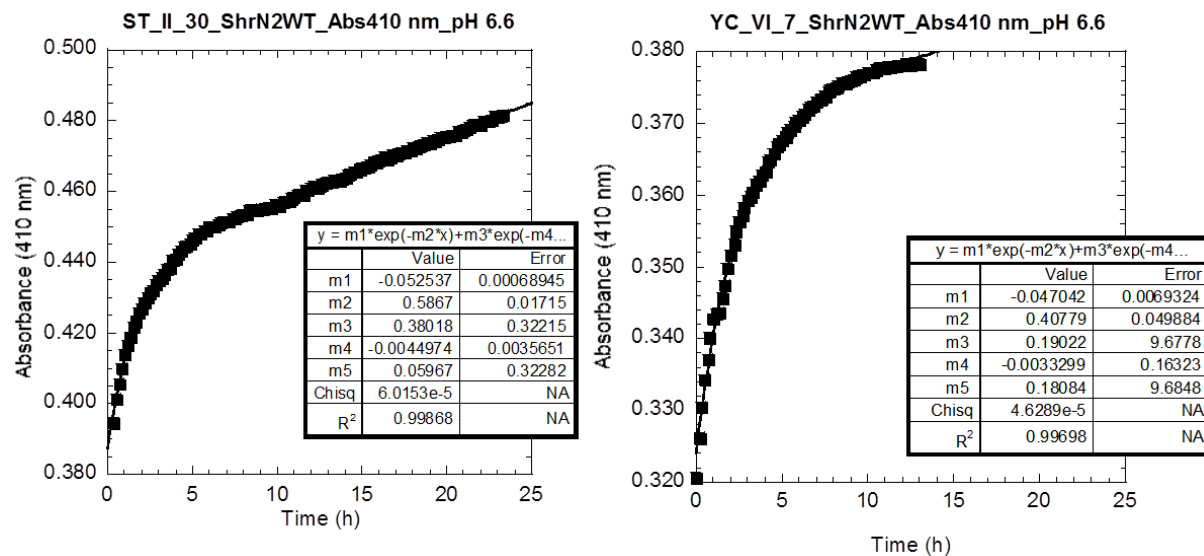


Figure 3.8 Timescale of ST Shr-N2. Data fit at 410 nm.

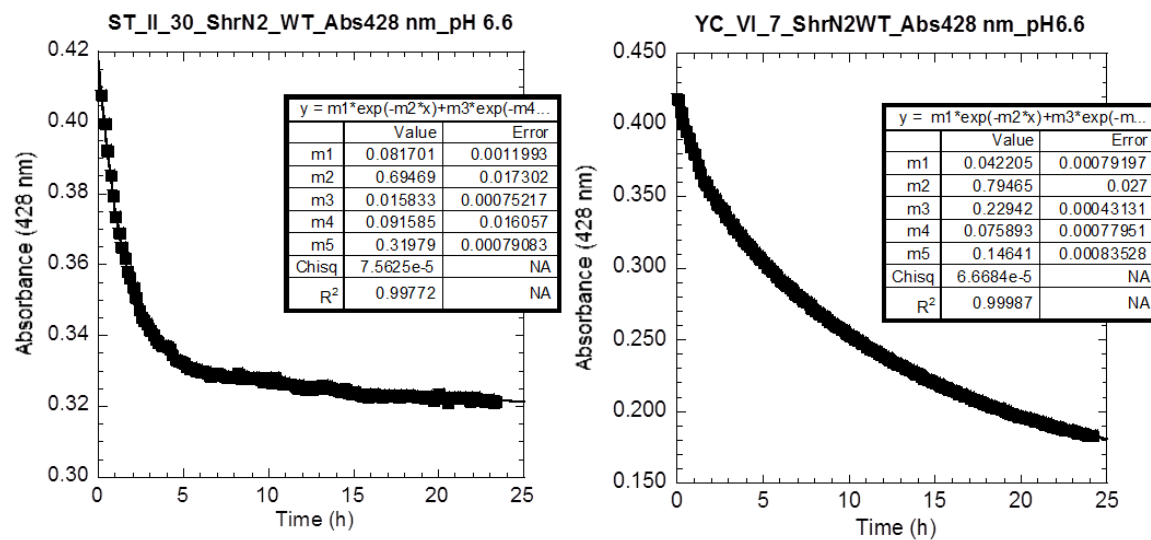


Figure 3.9 Timescale of ST Shr-N2. Data fit at 428 nm

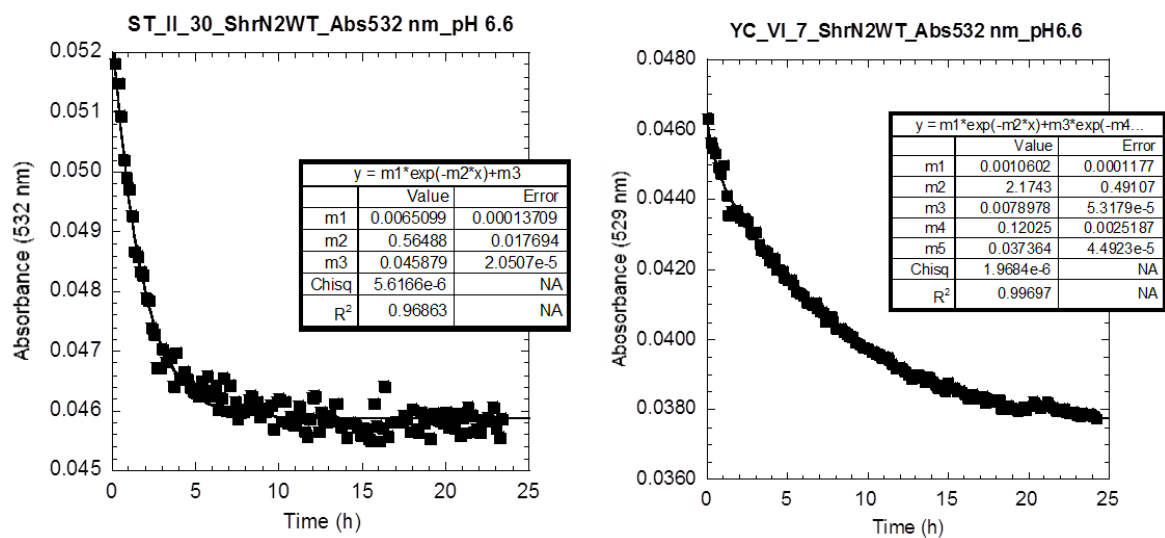


Figure 3.10 Timescale of ST Shr-N2. Data fit at 532 nm

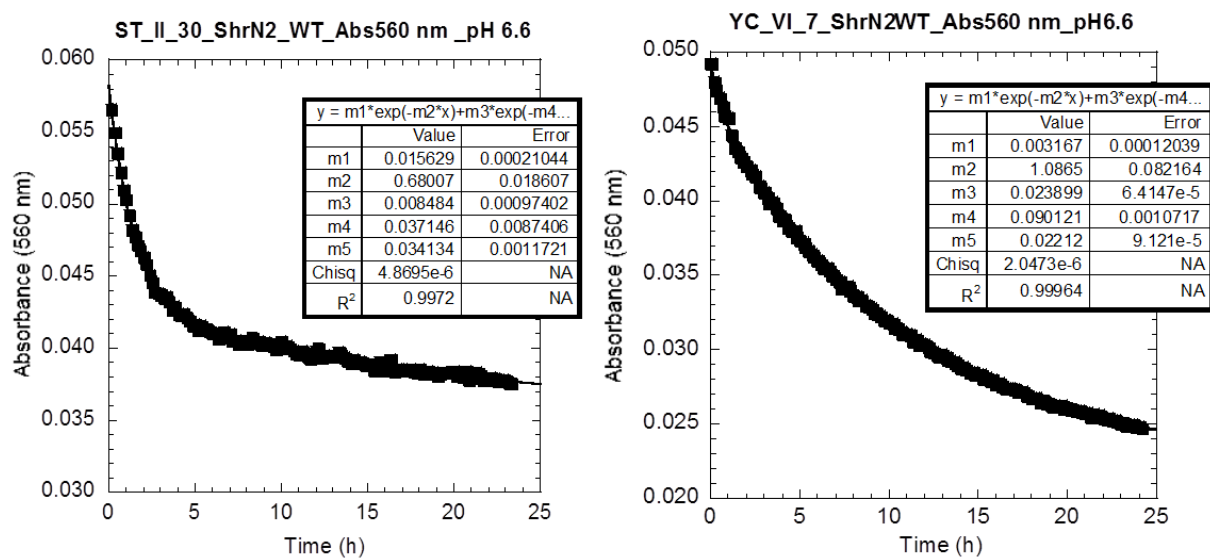


Figure 3.11 Timescale of ST Shr-N2. Data fit at 560 nm

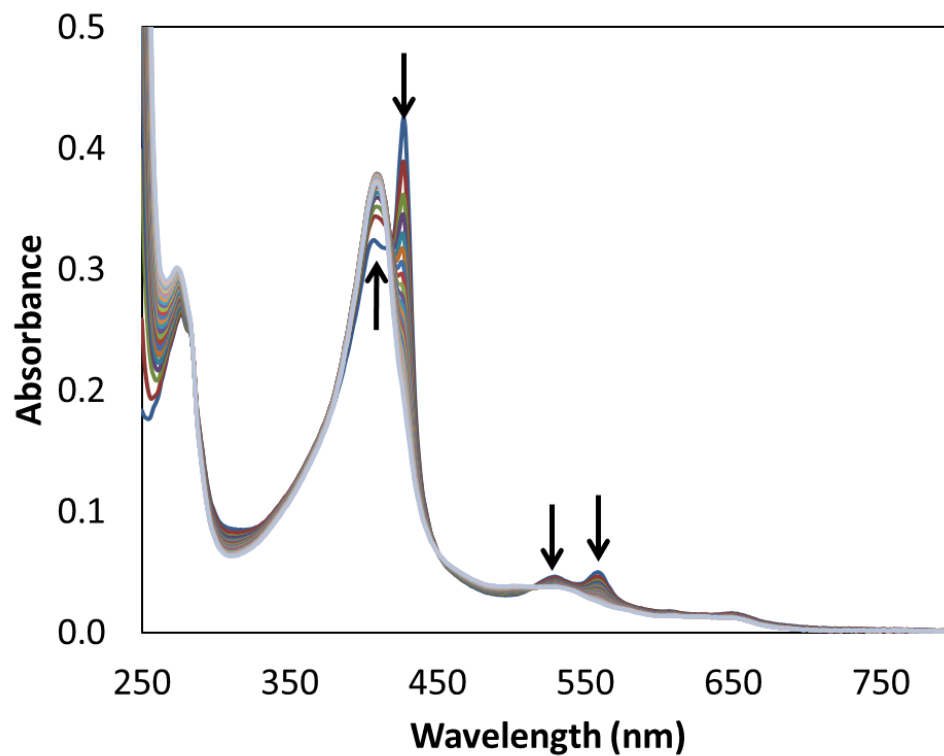


Figure 3.12 YC_VI_7. Absorbance vs. wavelength over 24 h for a solution of WT ShrN2 in 20 mM CAPS, MES, and Tris-Cl at pH 6.6. The pH of the sample was adjusted from 10.4 to 6.6 using 1 M HCl. The absorbance at 428 nm decreases while that at 410 nm increases. The α,β bands decrease. Data recorded by Yu Cao.

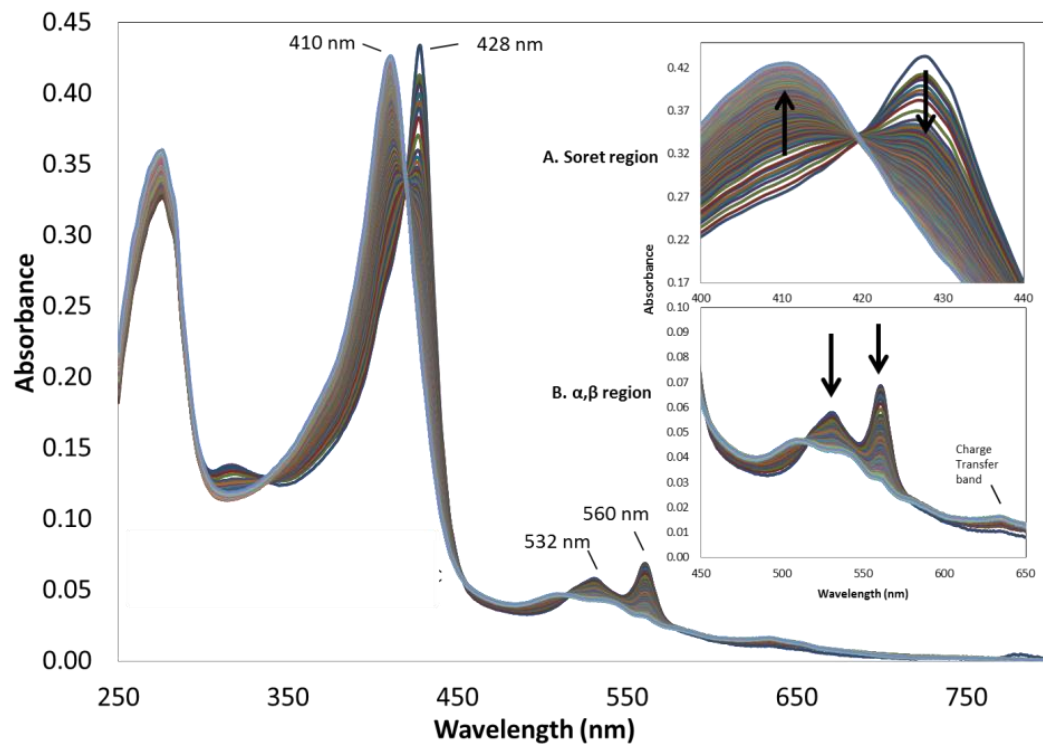


Figure 3.13 Autoxidation of WT Shr-N2 pH 6.1. Sample prepared in TE buffer (10 mM Tris-Cl, 1 mM EDTA pH 8.0). 1 M HCl added to take pH down to 6.1. Spectra followed every 10 min for 24 h. Arrows indicate the increasing and decreasing peaks over time.

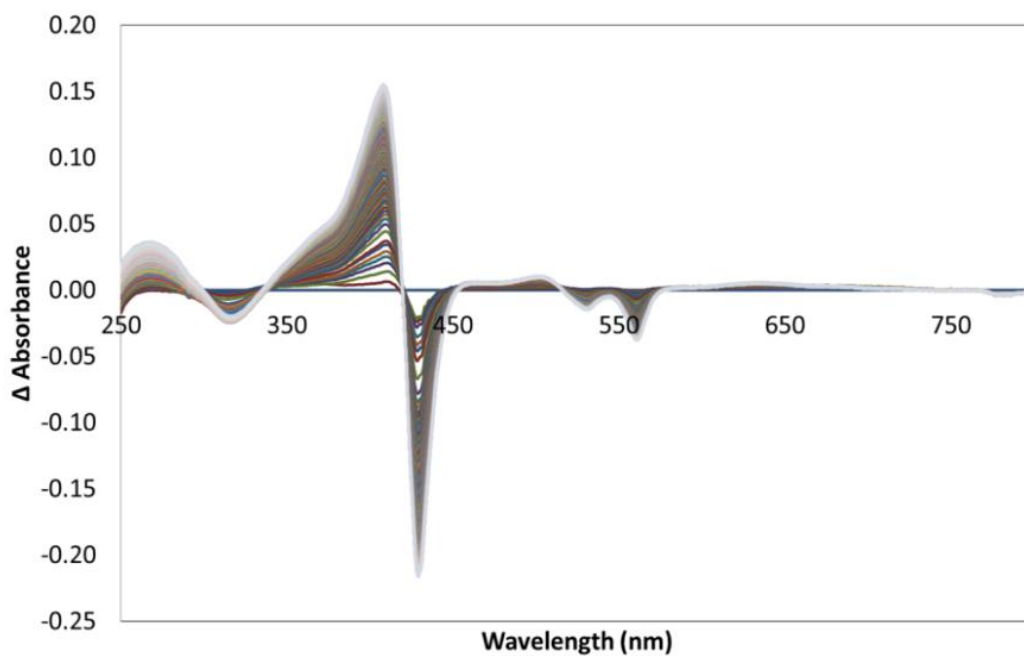


Figure 3.14 Difference spectra for autoxidation of WT Shr-N2 at pH 6.1.

3.8.2 pH Dependent Autoreduction of WT Shr-N2

Yu Cao's sample described above was then adjusted to pH 10.5 with 1.0 M NaOH and followed for 24 h. The protein reduced in a process largely complete in about 2 h. The same then began to autoxidize again, a process that was not complete in 24 h (Figure 3.15). Fitting to a biphasic process was not successful. Overall, changes as a function of pH were only partially reversible, with significantly less protein available to reduce after a reduction-oxidation cycle (Figures 3.8-3.11). As seen in Yu Cao's data, at high pH after a 24 h span, the proteins spectra is consistent with precipitation or denaturation. Data at pH 10.5 could not be fit.

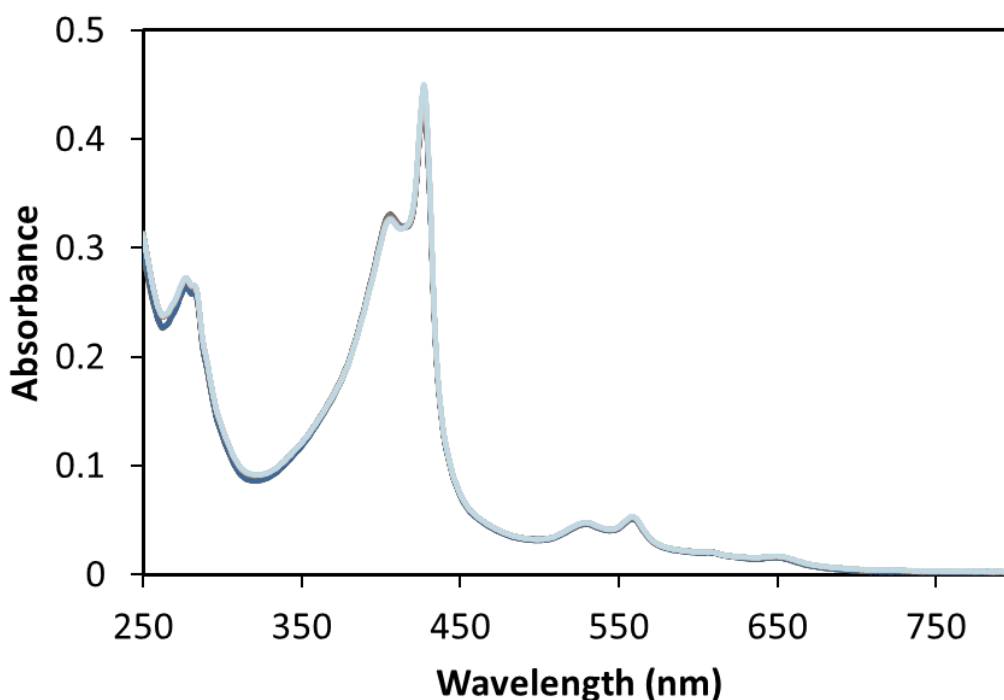


Figure 3.15 . Absorbance vs. wavelength over 18 h for a solution of WT ShrN2 in 20 mM CAPS, MES, and Tris-Cl at pH 10.4. The pH of the sample was adjusted to 10.4 using 1 M NaOH. The absorbance at 428 nm increases while that at 406 nm decreases. The α, β bands decrease. Data recorded by Yu Cao.

The new sample of protein from the same stock solutions was prepared for WT Shr. The pH of the sample was adjusted to 10.5 and spectra were taken over time. Figure 3.16 shows the spectra over time along with the difference spectra in Figure 3.17. The lack of isosbestic points leads to conclude that more than one intermediate is present in solution. The absorbance of WT both increased and decreased over time. Rate constant fittings at those wavelengths have a greater margin of error as a result. Only the reductive branch of the data set could be fit in KaleidaGraph to obtain approximate rate constants for WT Shr. Data not shown.

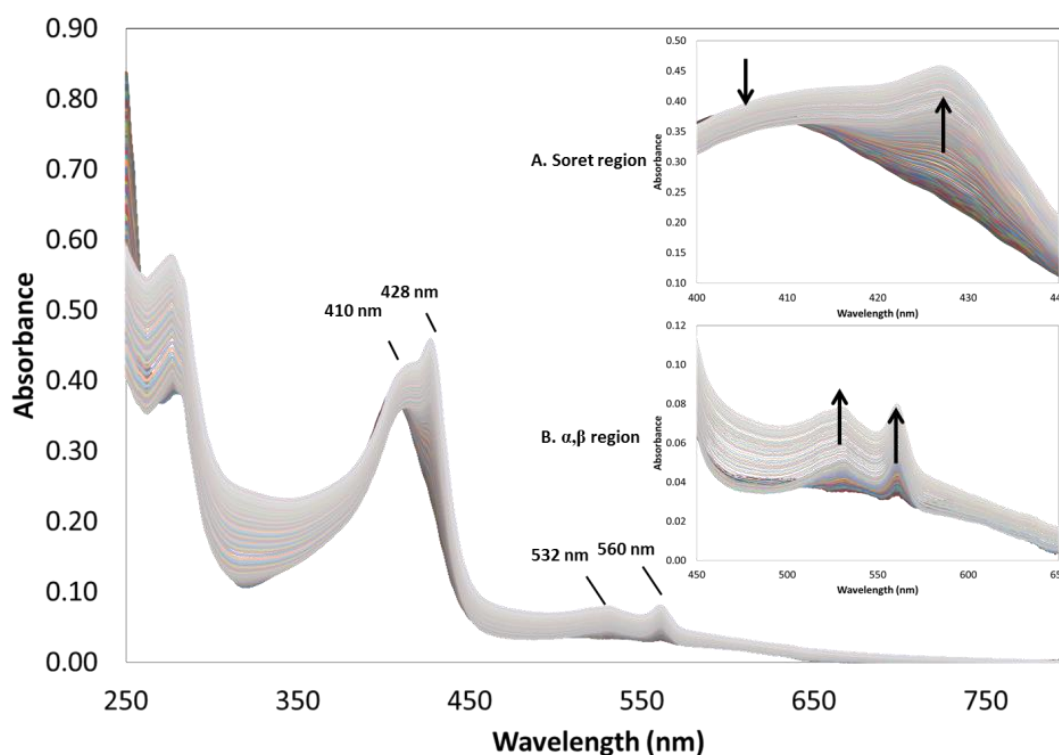


Figure 3.16 Autoreduction of WT Shr-N2 at pH 10.5. Sample prepared in TE buffer (10 mM Tris-Cl, 1 mM EDTA pH 8.0). To the sample, 1 M NaOH was added to take pH up to 10.5. Spectra followed every minute for 2 h then every 10 min for 22 h.

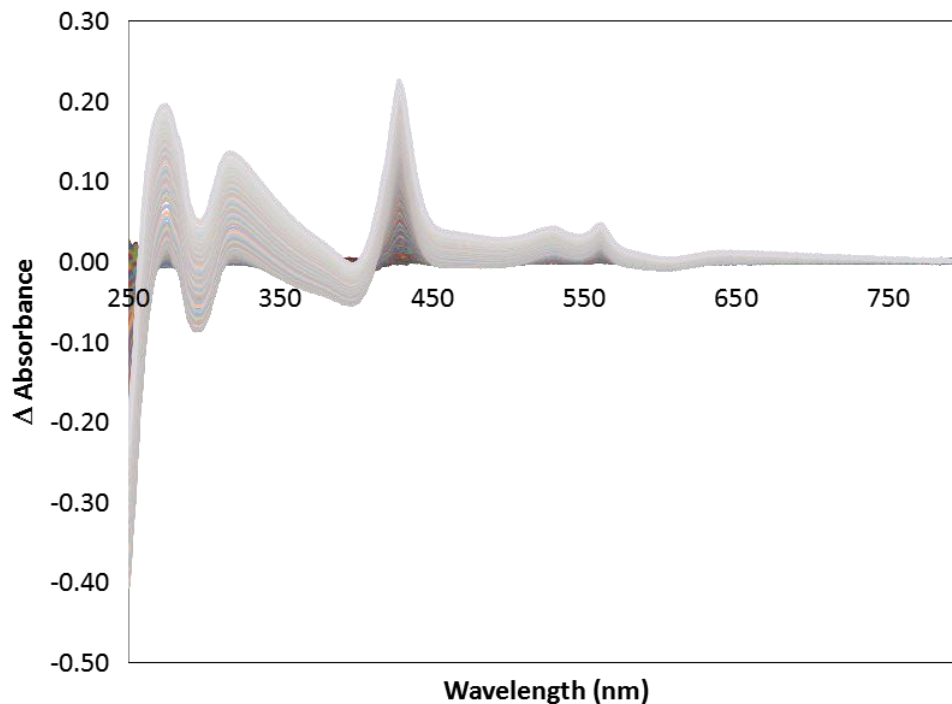


Figure 3.17 Difference spectra for autoreduction of WT Shr-N2 at pH 10.5.

There are two possibilities that may be contributing to this occurrence. If lysine is involved in autoreduction, each cycle probably destroys the lysines involved. Therefore, an “autoreduced” sample may already have “lost” at least one lysine. Another possibility is that the methionine residue can have two orientations with respect to the heme, essentially “R” and “S” conformations. Therefore, a bis-methionine protein can have four different conformational states. These orientation possibilities have been studied for some of the cytochrome *c*⁶⁸. Based on the data shown, there is no consistency among the rate constants and in comparison at low and high pH. In solution there are multiple processes occurring giving rise to unstable behavior.

4 CHAPTER 3: THE DNA TRANSCRIPTION REGULATOR PEFR IN *STREPTOCOCCUS PYOGENES*

4.1 Multiple antibiotic resistance regulators and porphyrin-regulated efflux via PefR

Streptococcus pyogenes causes many human diseases including strep throat, pharyngitis (rheumatic fever), toxic shock syndrome, necrotizing fasciitis, and joint or bone infections. Antibiotic resistance is a growing concern⁷⁰⁻⁷². Because this organism uses heme as an iron source,⁷³ control of proteins that bind and transport heme is of interest. Recently, the Eichenbaum laboratory performed microarray analysis of the transcription response to heme exposure in the Group A Streptococcus (GAS) genome⁴⁸. The porphyrin regulated efflux (pef) regulon consists of gene clusters *pefAB* and *pefRCD* that code for transporter proteins (*pefAB*, *pefCD*)⁷⁴. In particular, a porphyrin-regulated efflux protein PefR was discovered. PefR controls the expression of these iron-regulated proteins. PefR has a molecular mass of 17.4 kD with a theoretical pI of 9.2. In GAS it is thought that increased levels of heme or PPIX activates transcription by releasing PefR from its promoter region upon heme or PPIX binding⁴⁸.

The structure of PefR, based on homology modeling, belongs to the family of Multiple antibiotic resistance regulators (MarR) proteins. MarR are negative regulators encoded by the *marRAB* locus in *E. coli*. This regulation family controls the expression of proteins resulting in resistance to conventional antibiotics⁷⁵. Roughly 100 MarR-like proteins have been characterized to date, in which many bind to their individually associated DNA. Structurally, MarR proteins are found as dimers. They are α -helix-rich; the N- and C- termini form a dimer domain that is stabilized by hydrophobic interactions. MarR proteins have a helix-turn-helix motif, common in DNA binding. It is composed of two helices joined by a short strand. The first helix is the recognition helix. The second helix is known to be the stabilizing helix which

interacts with the DNA itself and therefore stabilizes helix one via hydrophobic interactions. Results from the Protein Data Bank show many topologically similar proteins from different organisms such as *P. aeruginosa*, *B. subtilis* and *E. faecalis*. Although the family has low sequence identity (~ 20%), most of the structures are very similar in three dimensions. MarR-like proteins bind to lipophilic compounds. MarR proteins bind to DNA in the apo form and are released from the DNA in the holo form. Following the general pattern of MarR proteins, PefR is thought to exist as a dimer which releases itself from the promoter region upon binding heme. This release leads to the repression of the two heme export systems *pefRCD* and *pefAB*.

The goal of the current study was to determine the axial ligand(s) bound to the hemin in the holo form of the protein, verify the stoichiometry of hemin binding, and create pure protein for future DNA binding studies. The previous construct of PefR used a histidine tag⁴⁸. Because the histidine tag can bind hemin,^{76,77} we have used a Strep-tag in our work.

4.2 Materials and Methods

4.2.1 WT PefR Protein Transformation

All water was 18 mΩ from a Barnstead water purifier. *E. coli* BL21 DE3 (New England BioLabs) cell line was used to transform WT PefR plasmid, designed by Rizvan Uluisik and prepared by Novagen. The plasmid (1 μL) and competent cells (50 μL) were incubated in a microcentrifuge tube on ice for 20 min. The solution was heat shocked in a water bath at 42 °C for 45 sec, then immediately placed back on ice for 2 min. The solution (51 μL) was added to warm LB media (250 μL) and left to shake at 37 °C for 1 h. The sample was then streaked onto agar plates with kanamycin (50 μg/mL) and incubated overnight at 37 °C. One colony was chosen and half was grown in LB media (10 mL) for DNA extraction. The other half of the

same colony was used to streak a new plate. Once the DNA was extracted, it was sent to be sequenced at GENEWIZ.

4.2.2 *WT PefR Protein Expression*

LB media was prepared (10 g of tryptone, 10 g of NaCl, 5 g of yeast extract, 1 L of Barnstead Diamond Nanopure water) in three 2 L flasks. The media was sterilized on a 20 min cycle. After cooling to room temperature, 500 μ L of 100 mM kanamycin stock solution was added to each 2 L flask. To separate 125 mL flasks, 25 mL of the broth containing kanamycin was extracted and inoculated with a WT PefR glycerol stock solution, using the sterile flame loop technique. All flasks were incubated for approximately 18 h. The contents were then returned to the 2 L flasks containing the remaining LB solution, to allow for growth on a larger scale. Using a Varian 50 Bio UV-visible spectrophotometer, the optical density OD₆₀₀ was taken. The media was induced with 1 mL of 100 mM isopropyl β -D-1-thiogalactopyranoside (IPTG), once the absorbance reached an OD₆₀₀ between 0.6 and 0.8 (approximately 4 h). The temperature was reduced to 27 °C and the media continued shaking for another 18 h. The cells were harvested using a JLA 8.100 rotor Beckman Coulter Avanti-T26 XPI centrifuge at 8,000 G for 30 min at 4 °C. The cell pellet (15 g) was extracted and stored at 80 °C.

4.2.3 *WT PefR Protein Purification*

WT PefR cell pellet was placed in a beaker on ice containing buffer A (100 mM Tris-Cl 150 mM NaCl), 100 mM magnesium chloride, 10 mM phenylmethylsulfonyl fluoride, 10 mg/mL lysozyme, 5 μ g/mL each of DNase I Recombinant (Roche Diagnostics, Lot 14636800) and RNase A (Roche Diagnostics, Lot 70297724) from bovine pancreas, and 500 mM NaCl. The sample was lysed on ice for 30 min. The settings were set to 10 sec pulse on time and 10 sec

pulse off time with an amplitude of 19%. Once lysed, the sample was centrifuged at 7000 rpm for 45 min at 4 °C. The supernatant was collected and stored (-80 °C).

The purification steps were conducted at 4 °C using a GE Healthcare ÄKTA FPLC; all buffer solutions were adjusted to pH 8.0. The sample (one Falcon tube) was loaded onto a Strep-Tactin Superflow column (5 mL, IBA BioTAGnology) equilibrated with buffer A (100 mM Tris-HCl, 150 mM NaCl, pH 8.0). Unbound material was washed out with 5 column volumes (CV) of buffer A. The protein was eluted with 10 CV of buffer B containing 100 mM Tris-HCl, 150 mM NaCl, 2.5 mM desthiobiotin, pH 8.0 applied via a linear gradient. This sample was stored in the -80 °C freezer.

His-tagged PefR, purified from the construct developed in the Eichenbaum laboratory,⁴⁸ was a kind gift of BeiBei Liu from the laboratory for Dr. W. David Wilson.

4.2.4 Bradford Assay WT PefR

A 5 µM stock solution of bovine serum albumin was prepared in water. The spectrophotometer was blanked with 200 µL of Coomassie Brilliant Blue G-250 dye (pre-made solution from Thermo Scientific) and 800 µL water. Solutions of BSA from 0.012 to 0.06 µM were prepared in duplicate. Dye (200 µL) was added to sample which was then incubated for 5 min. Spectra were taken and averaged for each concentration. A sample of PefR in water was also treated similarly with Coomassie Brilliant Blue solution and the spectrum taken. Placement of this point on the linear regression plot of the BSA was used to calculate the unknown concentration.

4.2.5 Heme Titration of WT PefR

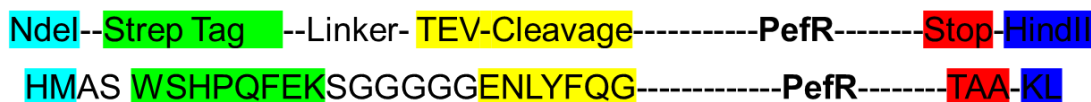
A 1 mL solution of WT PefR (5 µM as determined via Bradford Assay) was prepared in buffer A (150 mM NaCl, 100 mM Tris-Cl at pH 8.0). The hemin solution was prepared by

mixing 2 mg of hemin [ferriprotoporphyrin IX chloride (Fluka)] in 1 mL of DMSO. An extinction coefficient of heme in DMSO was used (heme $\epsilon_{404\text{ nm}}$ in DMSO $179\text{ mM}^{-1}\text{ cm}^{-1}$)⁷⁸. A 1,000-fold dilution was made and a spectra taken to calculate the concentration of the stock, solution which was 807 μM . The titration was carried out via a double cuvette system. One quartz cuvette was used as the blank containing 1 mL buffer A. The second cuvette contained 1 mL of the 5 μM protein solution. To each cuvette was added 1 μL of the hemin solution every 15 min. The spectrum was taken of protein heme solution, using the heme-only solution as the blank.

4.3 Results and Discussion

A construct of PefR with a Strep-tag was designed by Dr. Rizvan Uluisik and purchased from Novagen (Figure 4.1). Transformation was performed and the resulting gene sequenced.

Figure 4.2 shows that the correct sequence was obtained.



PefR Sequence

MSQVIGDLRELIHQIEQISDEIAKKYDVEHLAGPQGYVLVFLAKHQNQEIFVKDIEKQLRISKSVASHLVKRMVKN
 GFINVMPSQVDKRYKQVVLAQVGRDKLPLLRECRKDIEHYFLKEITKELLTAKKVIEQLKQNMLTYKGDNDA

Figure 4.1 Construct of PefR

PefR_ForA-pET_F_E02.ab1	NNNNNNNNNNNNNTCCNTCTAGAATAATTTTGTAACTTTAAGAAGGAGATATACATA	60
PefR_RIZFor-pET_F_E02.ab1	-----Cata	4

PefR_ForA-pET_F_E02.ab1	TGGCCAGCTGGAGCCACCCGAGTTCGAAAAGAGCGGTGGTGGTGGTAAAACTGT	120
PefR_RIZFor-pET_F_E02.ab1	tggccagctggagccacccgagttcgaaaagagcgggtgggtgggtgaaatctgt	64

PefR_ForA-pET_F_E02.ab1	ATTTCCAGGGTATGTCACAAGTGATAGGTGATTTACGTGAATTGATACATCAAATCGAAC	180
PefR_RIZFor-pET_F_E02.ab1	atttccaggtatgtcacaagtgatagtgatttacctgaattgatacatcaaatcgaac	124

PefR_ForA-pET_F_E02.ab1	AAATAGTGATGAGATTGCAAAAAAATATGATGTAGAGCATCTAGCAGGCTCTCAAGGTT	240
PefR_RIZFor-pET_F_E02.ab1	aaatagtgatgagattgcaaaaaaatatgatgtagagcatctagcaggtcctcaaggtt	184

PefR_ForA-pET_F_E02.ab1	ATGTTCTGTTTTTACGTAACACCAAAAATCAAGAAATATTTGTCAAAGATATTGAAA	300
PefR_RIZFor-pET_F_E02.ab1	atgttctgttttttagtcaaacacaaaatcaagaaatattgtcaagatattgaaa	244

PefR_ForA-pET_F_E02.ab1	AACAACCTCGTATCTCAAAGTCAGTTGCTAGTCATTTAGTGAAACGTATGGTCAAAAATG	360
PefR_RIZFor-pET_F_E02.ab1	aacaactcgtatctcaaagtcagttgctagtcatttagtgaacgtatggtcaaaaatg	304

PefR_ForA-pET_F_E02.ab1	GGTTTATCAATGTGATGCCTTCCAAGTGGATAAGCGTTATAAGCAAGTAGTGTAGCGC	420
PefR_RIZFor-pET_F_E02.ab1	ggtttatcaatgtgatgccttccaagtgataagcgttataagcaagtagttagcgc	364

PefR_ForA-pET_F_E02.ab1	AGGTTGGTAGAGATAAATTGCCTTTGTTGCGGGAGTGTGTAAGGATATCGAGCACTATT	480
PefR_RIZFor-pET_F_E02.ab1	agttgtagagataaattgcctttgttgcgggagtgctgaagatctgagcactatt	424

PefR_ForA-pET_F_E02.ab1	TTTTAAAAAAGAAATACAAAAGAAGAGTGTGACAGCGAAAAAAGTAATTGAACAGCTCA	540
PefR_RIZFor-pET_F_E02.ab1	ttttaaagaaattacaaaagaagagtgctgacagcgaaaaaagtaattgaacagctca	484

PefR_ForA-pET_F_E02.ab1	AGCAAAATATGCTAACTTATAAAGGAGACAACGATGCTTAAAGCTTGCAGCCGCACTCG	600
PefR_RIZFor-pET_F_E02.ab1	agcaaaatgctaactataaaggagacaacgatccttaaaagctt-----	531

PefR_RevA-pET_R_G02.ab1	GGTGGTGTGCTCGAGTGCAGCCGCAAGCTTTTAAAGCATCGTTGCTCCTTTATAAGTTA	120
PefR_RIZREV-pET_R_G02.ab1	-----aagcttttaagcatcgtgtctctttataagtta	35

PefR_RevA-pET_R_G02.ab1	GCATATTTGCTTGAGCTGTTCAATTACTTTTTTCGCTGTCAGCAACTCTCTTTGTAA	180
PefR_RIZREV-pET_R_G02.ab1	gcatatttgccttgagctgttcaattactttttcgtgctcagcaactctctttgttaa	95

PefR_RevA-pET_R_G02.ab1	TTTCTTTTAAAAAATAGTGTGCTCGATATCCTTACGACACTCCCAGCAAAAGGCAATTTAT	240
PefR_RIZREV-pET_R_G02.ab1	tttcttttaaaaaatagtgctcgatctccttacgacactcccgaacaaggaatttat	155

PefR_RevA-pET_R_G02.ab1	CTCTACCAACTGCGCTAACACTACTTGTCTATAACGCTTATCCACTTGGGAAGGCATCA	300
PefR_RIZREV-pET_R_G02.ab1	ctctaccaactgcgctaactactctgcttataacgcttatcacttgggaaggcatca	215

PefR_RevA-pET_R_G02.ab1	CATTGATAAACCCATTTTGGACATACGTTTCAATGACTAGCAACTGACTTTGAGA	360
PefR_RIZREV-pET_R_G02.ab1	cattgataaacccatTTTgaccatacgtttcactaaatgactagcaactgacttgaga	275

PefR_RevA-pET_R_G02.ab1	TACGAAGTTGTTTTCAATATCTTTGACAAATATTTCTTGATTTGGTGGTTAGCTAAAA	420
PefR_RIZREV-pET_R_G02.ab1	tacgaagtgttttcaatatcttgacaaatattcttgatttgggttttagctaaaa	335

PefR_RevA-pET_R_G02.ab1	AAACAAGAACATAACCTTGAGGACCTGTAGATGCTCTACATCATATTTTTGCAATCT	480
PefR_RIZREV-pET_R_G02.ab1	aaacaagaacataaaccttgaggacctgtagatgctctacatcatatTTTTTgcaatct	395

PefR_RevA-pET_R_G02.ab1	CATCACTAATTTGTCGATTTGATGATCAATTCACGTAATCACCTATCACTTGTGACA	540
PefR_RIZREV-pET_R_G02.ab1	catcactaatttgcgattgatgatcaattcacgtaaatcacctatcacttgtgaca	455

PefR_RevA-pET_R_G02.ab1	TACCCGGAATAACAGATTTTACCACCACCACCACCGCTCTTTTCAACTGCGGGTGGC	600
PefR_RIZREV-pET_R_G02.ab1	taccctggaataacagattttaccaccaccaccacgctcttttgaactcgggtggc	515

PefR_RevA-pET_R_G02.ab1	TCCAGCTGGCCATATGTATATCTCCTCTTAAAGTTAAACAAAATATTTCTAGAGGGGA	660
PefR_RIZREV-pET_R_G02.ab1	tccagctggccatG-----	531

Figure 4.2 Sequence alignment of PefR showing proper transformation of plasmid in cell line.

It is common for transcription factors to be isolated bound to DNA. Early experiments in our laboratory on PefR found this to be a significant issue. A study of successful transcription factor purifications by Cyrienne Keutcha of our laboratory showed a high salt concentration (500 mM NaCl) was added to the lysing step in almost every instance (Table 4.1).

Table 4.1 Purification techniques of DNA bound proteins.

Protein	PI/ Aromatic Residues	Lysis Buffer	Purification	Reference
Rv0678	5.69/(1W)(4Y)	200 mM sodium chloride 20mM Na-HEPES, pH 7.2 10 mM magnesium chloride 0.2 mg of DNase I	5 mL His-Trap Ni ²⁺ chelating column (GE Healthcare)	79
MarR	8.56/(1W)(1Y)	300 mM sodium chloride 10% glycerol 20 mM Tris-HCl pH 7.5 1 mM PMSF 5 mM β-mercaptoethanol	5 mL His-Trap column (GE Healthcare) Further purification step using HiLoad 16/60 Superdex 200 column (GE Healthcare)	80
PcaV	9.65/(1W)((2Y)	500 mM sodium chloride 50 mM Tris-HCl 5 mM imidazole 0.1% Triton X-100	His-Trap HP Ni ²⁺ affinity column (GE Healthcare)	81

When this protocol was followed, pure protein was isolated after FPLC on a Streptactin column as shown by SDS PAGE (Figure 4.3). Bradford analysis of the protein concentration allowed calculation of a total of 2.32 mg of protein isolated from a 3 L culture.

Heme proteins have a number of possible axial ligands, with His, Tyr, Met and Cys in general the most common⁸². Figure 4.4 highlights these residues in a homology model of PefR based on the MepR x-ray structure of this transcription factor bound to DNA⁸³. The alignment was obtained using I-TASSER⁸⁴.

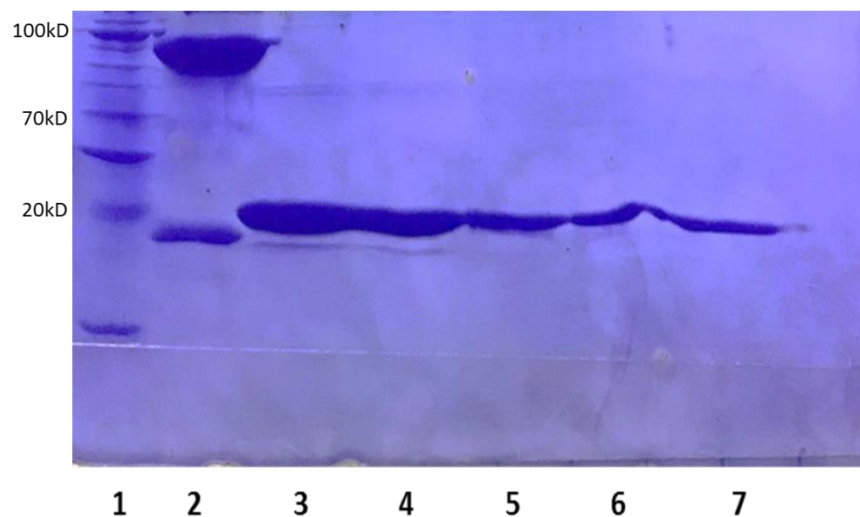


Figure 4.3 SDS gel of WT PefR elution. Lane 1. Protein Ladder. Lane 2. Mixed Ladder [BSA (66.5 kD), myoglobin (16.7 kD)]. Lane 3-7. Fractions containing PefR.

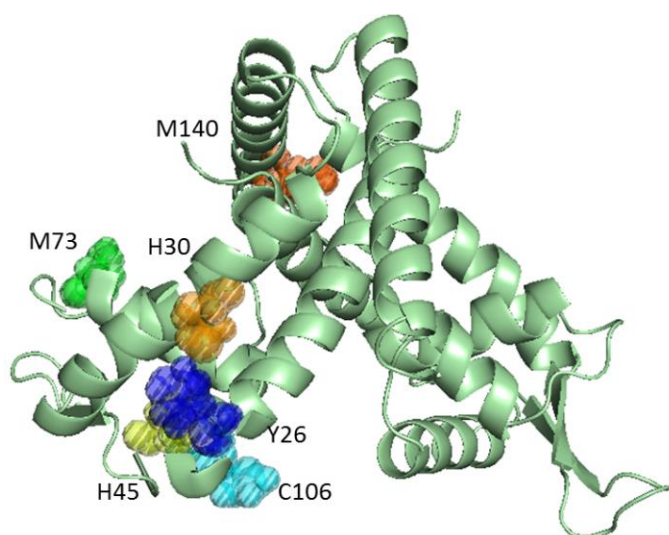


Figure 4.4 I-TASSER model of PefR showing potential axial ligands

The UV-visible absorbance spectrum (Figure 4.7) shows minimal heme loading. The extinction coefficient of the 280 nm band is low in PefR ($7,450 \text{ M}^{-1} \text{ cm}^{-1}$ as calculated from ExPASy⁸⁵) because this protein has no tryptophans in the sequence, only a single Trp in the Strep-tag. A useful rule of thumb is that the extinction coefficient of the heme in a heme protein is about $1 \times 10^5 \text{ M}^{-1} \text{ cm}^{-1}$ at the Soret. Given this, the Soret/280 absorbance ratio of 0.05 indicates that the as-isolated protein is about 5 % heme loaded. An expanded plot of the spectrum, (magnified 25 times) shows bands at 570, and 615 nm (Figure 4.7). These are consistent with a Cys axial ligand, as discussed in more detail below.

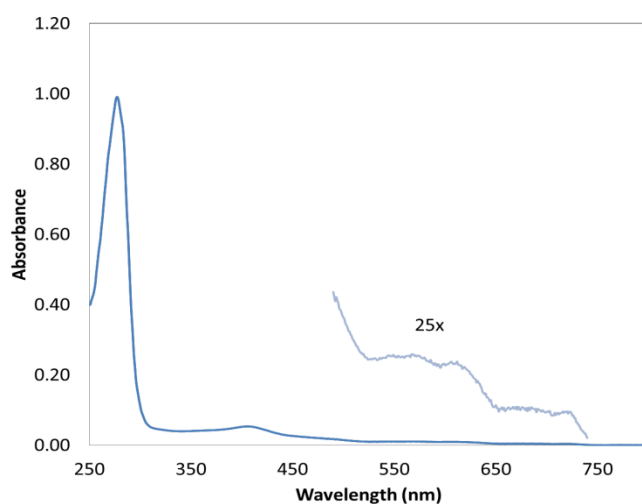


Figure 4.5 UV-visible absorption spectra of WT PefR.

A heme titration was conducted for PefR, in which aliquots of hemin in DMSO were added to two cuvettes, one with buffer only (blank) and one with a PefR solution. Figure 4.8 shows the absorbance as a function of the concentration of hemin. The absorbance of the Soret at 390 nm increases as function of added hemin, with a break in the slope at 1.25. It is probable that this indicates 1:1 hemin:protein binding, with the Bradford Assay not a completely reliable indicator of the true protein concentration. It is also possible that the baseline increase at lower

wavelengths, presumably due to light scattering is responsible for the discrepancy. The 390:280 nm absorbance ratio increases as the titration progresses, indicating hemin binding to the protein. Figure 4.9 plots this ratio as a function of the concentration of hemin. Again, a break point in the slopes is seen at a hemin:protein ratio of about 1.25, consistent with the data plotted using the 390 nm absorbance.

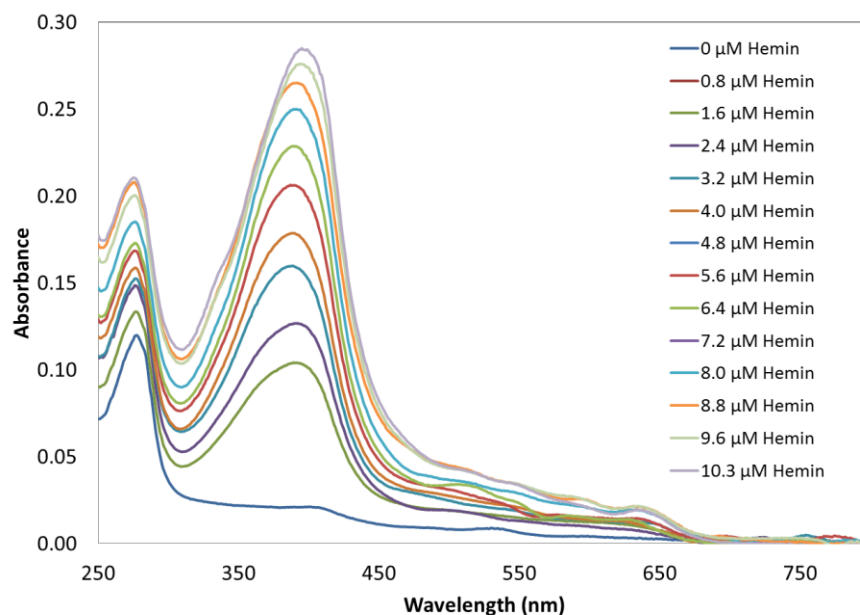


Figure 4.6 Heme Titration of PefR. Protein (5 μM) was prepared in 100 mM Tris-Cl, 150 mM NaCl pH 8.0. Hemin in DMSO (1 μL of an 807 μM stock) added every 15 min to both the solution of PefR and a blank containing buffer only. Spectra are shown as a function of the concentration of hemin.

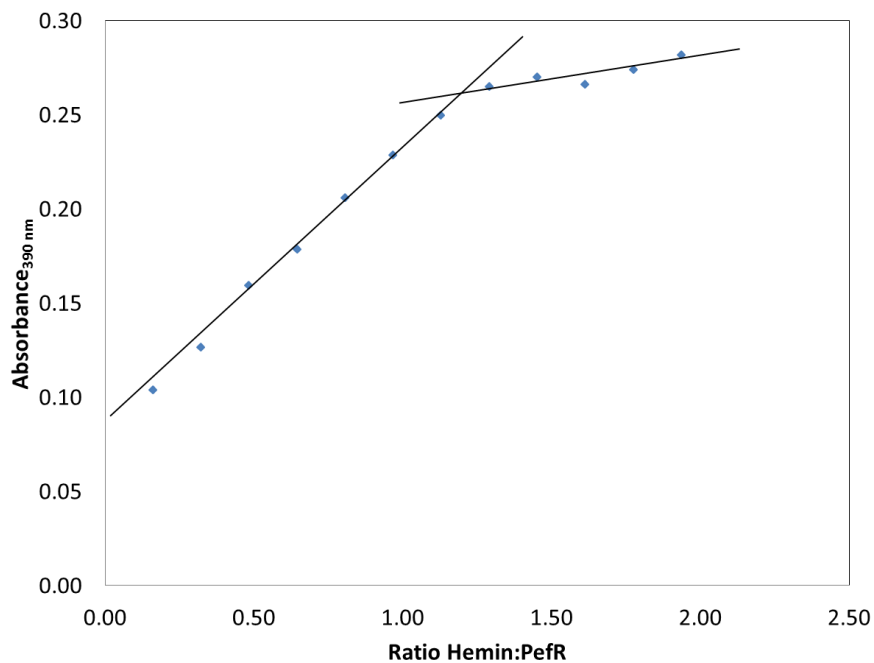


Figure 4.7 Absorbance at 390 nm as a function of the ratio of hemin to PefR.

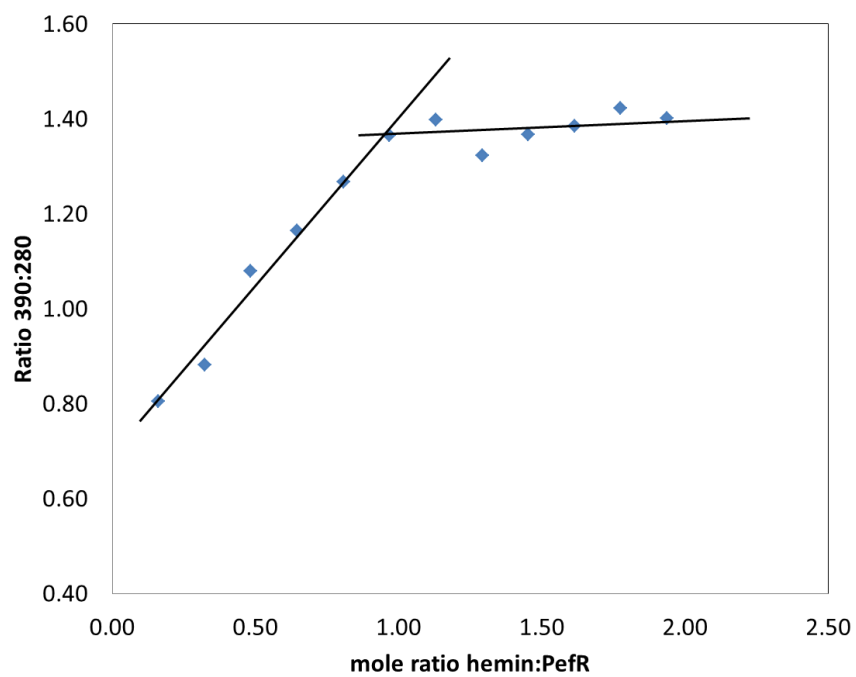


Figure 4.8 Ratio of the 390 nm to 280 nm bands as a function of the ratio of hemin to PefR

A recent review on heme binding transcription factors details the observation that cysteine (usually next to a proline) and histidine are the two most common ligands in heme-binding transcription factors⁸⁶. Cysteine alone as an axial ligand gives a Soret in the 370 – 390 nm region, as tabulated in work on the Bach 1 protein (Type 2) as shown in Table 4.2⁸⁷. In general, histidine, either in 5-coordinate or 6-coordinate binding patterns, gives a Soret band > 405 nm. In model studies, H39G Mb bound to β -mercaptoethanol is a five-coordinate high-spin ferric center with a Soret at 390 nm and small α,β bands around 510 nm⁸⁸. Both of these are true for PefR. Thus, comparison of PefR spectra with literature data indicates that PefR has a Cys heme ligand, consistent with other studies on heme-bound transcription factors⁸⁶.

Table 4.2 Comparison of Bach1 to other heme proteins. Taken from⁸⁷

Heme proteins and models	Ligands	Soret (nm)	Visible (nm)	Reference
Bach1 (Type1)	Cys/His	423	540, 580	This study
Bach1 (Type2)	Cys	371	521, 541, 650	This study
P450 _{cam} (+cam) ^a	Cys	391	520, 540, 646	(25, 26)
P450 _{cam} (H ₂ O)	Cys/H ₂ O	417	536, 569	(27)
P450 _{cam} (Im) ^b	Cys/Im	425	542, 574	(28)
CBS ^c	Cys/His	428	550	(29)
CooA	Cys/Pro ^f	424	541, 566	(30, 31)
Cytb ₅ ^d	His/His	413	532, 560	(32)
Irr ^e	Cys	377	ND ^g	(2)
Heme + Peptide (AKRCPADHTM)	Cys	362	ND ^g	(12)
Heme dimethyl ester + <i>p</i> -nitrobenzenethiol	SC ₆ H ₄ NO ₂	386	517, 540, 649	(33)

^aP450_{cam}(+cam), *d*-camphor bound P450_{cam}; ^bP450_{cam} (Im), imidazole bound P450_{cam}; ^cCBS, cystathionine- β -synthase; ^dCytb₅, cytochrome b₅; ^eIrr, iron response regulator protein; ^fPro, N-terminal Proline binds to heme; ^gND, not determined.

Previous work on PefR used a His-tagged protein⁸⁹. Because histidine is an excellent ligand for heme, there is a chance that it participates in binding to the heme of a His-tagged protein^{76, 77}.

Concerned about this possibility, we used a Strep-tagged construct. Figure 4.9 shows an overlay of the two spectra, normalized to 1.0 at the Soret. The blue absorbance spectrum represents his-tagged PefR. There is a large Soret peak appearing at 407 nm. There is a shoulder peak at 350

nm and α,β bands at 540 and 560, and 665 nm. This is a clear indication that the His-tag is interfering with heme binding resulting in a completely different spectra.

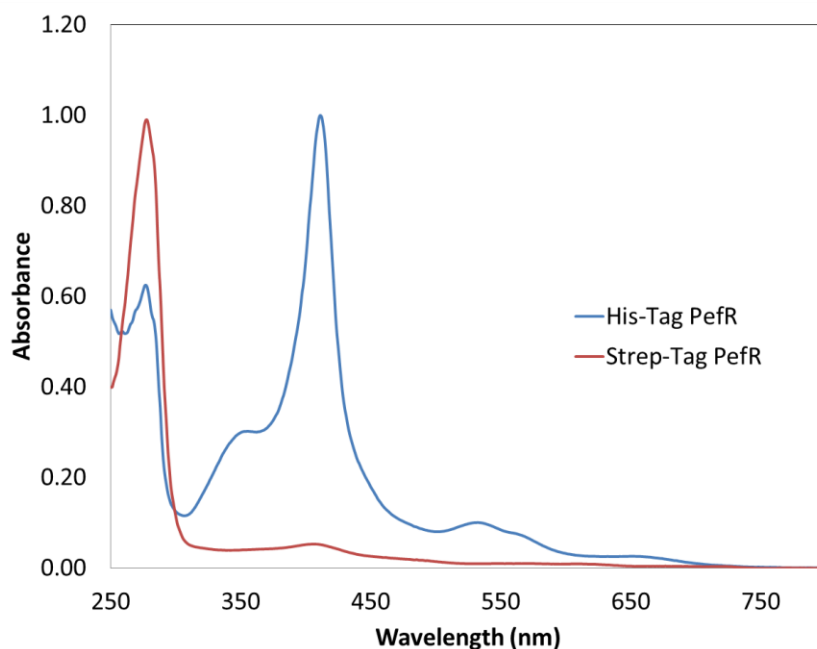


Figure 4.9 UV-visible absorption spectra of WT PefR. The blue spectrum is his-tagged PefR. The red spectrum is strep-tagged PefR.

To our knowledge, there is at present only one x-ray structure of a MarR transcription factor bound to DNA, MepR from *Staphylococcus aureus* (PDB 4LLL)⁸³. Figure 4.11 shows this structure with the residue homologous to PefR C106 (MepR I106) highlighted in blue. Heme binding could then produce a significant change in the three-dimensional structure of the protein, resulting in loss of DNA association when hemin binds to the protein. As an example of this type of structure change on heme binding is shown in Figure 4.10, in which the protein, HrtR, without heme (and bound to DNA) has a significantly different three-dimensional structure than the protein with heme bound (which does not bind to DNA)⁸⁶.

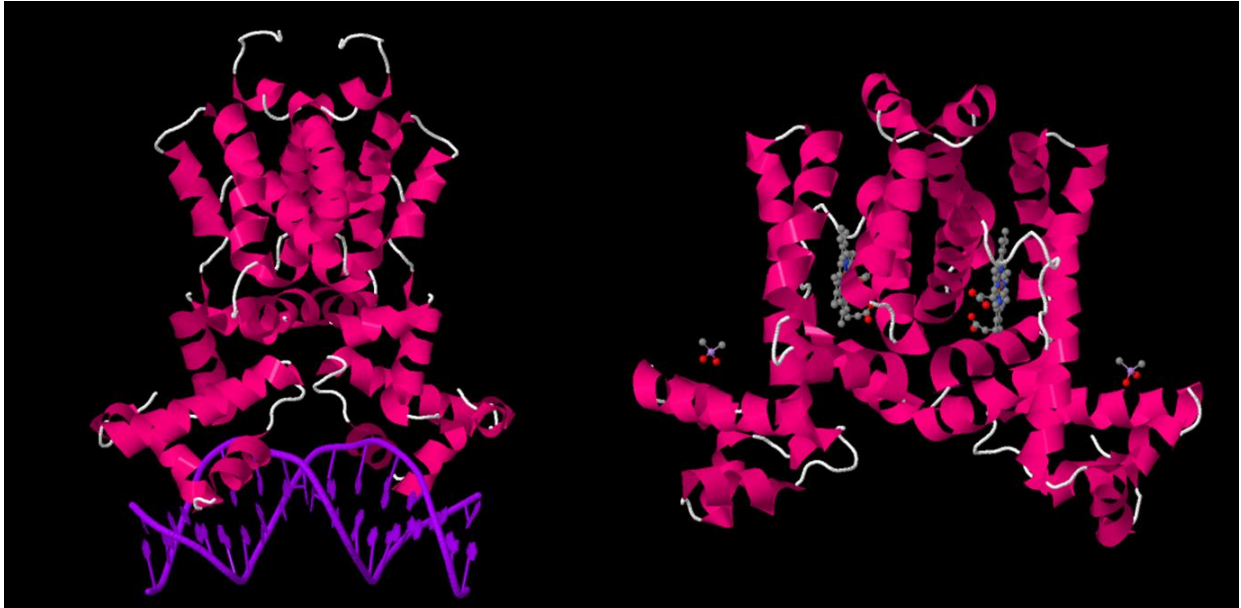


Figure 4.10 WT HrtR in the apo form with DNA (left PDB 3VOK) and holo form (right PDB 3VP5) ⁹⁰.

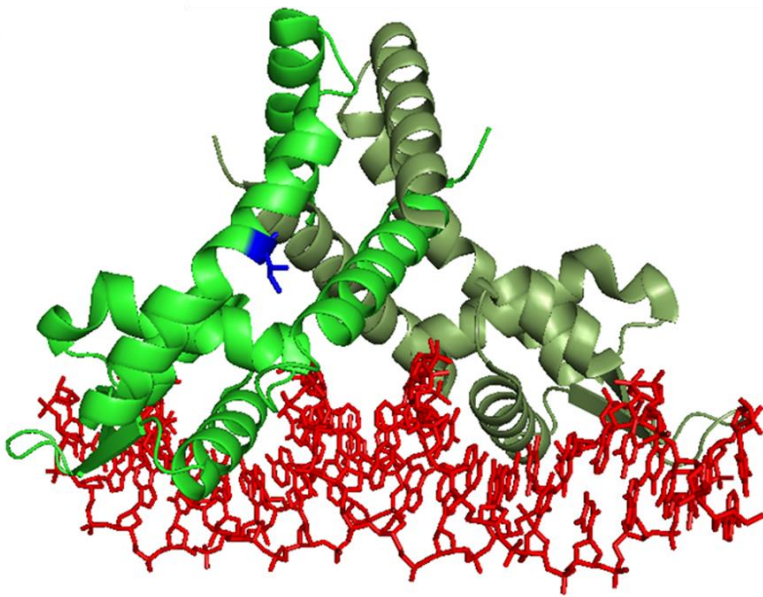


Figure 4.11 Crystal structure of *S. aureus* MepR bound to DNA 72. Highlighted in blue is residue I106, which corresponds to C106 in PefR, the putative heme axial ligand.

Conclusions

The spectrum is consistent with a Cys axial ligand. Hemin titration experiments indicate approximate 1:1 hemin:protein binding. Homology modeling predicts that C106 lies between

two α -helices. Heme binding would be expected to alter the three-dimensional structure of the protein significantly, allowing the expected pattern of the transcription factor binding to DNA without heme and being released from DNA when heme is bound.

4.4 General Conclusions

Most bacteria require iron and many pathogenic bacteria use hemin as the main source of iron during infections. Because free hemin is toxic, bacteria have developed regulatory mechanisms to control the expression of proteins used in heme binding and transport. In Group A *Streptococcus*, heme exposure results in a global transcriptome shift, up-regulating genes involved in redox stress⁴⁸. Determining how heme-binding transcription factors control gene expression is key in understanding the fundamental biochemistry of this pathway and may be significant in developing new therapeutic approaches to combat disease caused by this organism. Our studies on PefR reveal for the first time that this protein binds heme through a cysteine ligand, and provide a basis in terms of spectral data and heme binding ratios for future work in this area.

REFERENCES

- [1] Farrand, A. J., and Skaar, E. P. (2014) Heme and infectious diseases, In *Handbook of Porphyrin Science with Applications to Chemistry, Physics, Materials Science, Engineering, Biology and Medicine, Vol 26: Heme Biochemistry* (Ferreira, G. C., Kadish, K. M., Smith, K. M., and Guillard, R., Eds.), pp 317-377, World Scientific, Hackensack, NJ.
- [2] Benson, D. R., and Rivera, M. (2013) Heme uptake and metabolism in bacteria, *Met. Ions Life Sci.* 12, 279-332.
- [3] Rodgers, K. R., and Lukat-Rodgers, G. S. (2014) Biophysical perspectives on the acquisition, transport, and trafficking of heme in bacteria, *Handbook of Porphyrin Science with Applications to Chemistry, Physics, Materials Science, Engineering, Biology and Medicine, Vol. 30: Heme Proteins, Part II* 30, 249-309.
- [4] Wandersman, C., and Delepelaire, P. (2004) Bacterial iron sources: From siderophores to hemophores, *Annu. Rev. Microbiol.* 58, 611-647.
- [5] Edelstein, S. J., Rehmar, M. J., Olson, J. S., and Gibson, Q. H. (1970) Functional aspects of the subunit association-dissociation equilibria of hemoglobin, *J. Biol. Chem.* 245, 4372-4381.
- [6] Antonini, E., and Brunori, M. (1971) *Hemoglobin and Myoglobin in their Reactions with Ligands*, Vol. 21, North-Holland Publishing Company, Amsterdam.
- [7] Fermi, G., and Perutz, M. F. (1981) *Haemoglobin and myoglobin*, Clarendon Press, Oxford.
- [8] Bassetti, M., Merelli, M., Temperoni, C., and Astilean, A. (2013) New antibiotics for bad bugs: where are we?, *Ann. Clin. Microbiol. Antimicrob.* 12.
- [9] Smith, A. D., and Wilks, A. (2012) Extracellular heme uptake and the challenges of bacterial cell membranes, *Curr. Top. Membr.* 69, 359-392.
- [10] Mazmanian, S. K., Skaar, E. P., Gaspar, A. H., Humayun, M., Gornicki, P., Jelenska, J., Joachmiak, A., Missiakas, D. M., and Schneewind, O. (2003) Passage of heme-iron across the envelope of *Staphylococcus aureus*, *Science* 299, 906-909.
- [11] Torres, V. J., Pishchany, G., Humayun, M., Schneewind, O., and Skaar, E. P. (2006) *Staphylococcus aureus* IsdB is a hemoglobin receptor required for heme iron utilization, *J. Bacteriol.* 188, 8421-8429.
- [12] Bates, C. S., Montañez, G. E., Woods, C. R., Vincent, R. M., and Eichenbaum, Z. (2003) Identification and characterization of a *Streptococcus pyogenes* operon involved in binding of hemoproteins and acquisition of iron, *Infect. Immun.* 71, 1042-1055.
- [13] Lei, B. F., Smoot, L. M., Menning, H. M., Voyich, J. M., Kala, S. V., Deleo, F. R., Reid, S. D., and Musser, J. M. (2002) Identification and characterization of a novel heme-associated cell surface protein made by *Streptococcus pyogenes*, *Infect. Immun.* 70, 4494-4500.
- [14] Drazek, E. S., Hammack, C. A., and Schmitt, M. P. (2000) *Corynebacterium diphtheriae* genes required for acquisition of iron from haemin and haemoglobin are homologous to ABC haemin transporters, *Mol. Microbiol.* 36, 68-84.
- [15] Schmitt, M. P. (2004) *Corynebacterium diphtheriae*, In *Iron Transport in Bacteria* (Crosa, J. H., Mey, A. R., and Payne, S. M., Eds.), pp 344-359, ASM Press, Washington, DC.

- [16] Contreras, H., Chim, N., Credali, A., and Goulding, C. W. (2014) Heme uptake in bacterial pathogens, *Curr. Opin. Chem. Biol.* 19, 34-41.
- [17] Davidson, A. L., and Maloney, P. C. (2007) ABC transporters: How small machines do a big job, *Trends Microbiol.* 15, 448-455.
- [18] Takahashi, S., Wang, J. L., Rousseau, D. L., Ishikawa, K., Yoshida, T., Takeuchi, N., and Ikeda-saito, M. (1994) Heme-heme oxygenase complex - Structure and properties of the catalytic site from resonance Raman scattering, *Biochemistry* 33, 5531-5538.
- [19] Schmitt, M. P. (1997) Utilization of host iron sources by *Corynebacterium diphtheriae*: Identification of a gene whose product is homologous for eukaryotic heme oxygenases and is required for acquisition of iron from heme and hemoglobin, *J. Bacteriol.* 179, 838-845.
- [20] Trost, E., Blom, J., Soares, S. D., Huang, I. H., Al-Dilaimi, A., Schroder, J., Jaenicke, S., Dorella, F. A., Rocha, F. S., Miyoshi, A., Azevedo, V., Schneider, M. P., Silva, A., Camello, T. C., Sabbadini, P. S., Santos, C. S., Santos, L. S., Hirata, R., Mattos-Guaraldi, A. L., Efstratiou, A., Schmitt, M. P., Hung, T. T., and Tauch, A. (2012) Pangenomic study of *Corynebacterium diphtheriae* that provides insights into the genomic diversity of pathogenic isolates from cases of classical diphtheria, endocarditis, and pneumonia, *J. Bacteriol.* 194, 3199-3215.
- [21] Schmitt, M. P., and Drazek, E. S. (2001) Construction and consequences of directed mutations affecting the hemin receptor in pathogenic *Corynebacterium species*, *J. Bacteriol.* 183, 1476-1481.
- [22] Draganova, E. B., Akbas, N., Adrian, S. A., Lukat-Rodgers, G. S., Collins, D. P., Dawson, J. H., Schmitt, M. P., Rodgers, K. R., and Dixon, D. W. (2015) Heme binding by *Corynebacterium diphtheriae* HmuT: Function and heme environment, *Biochemistry* 54, 6598-6609.
- [23] Ekworomadu, M. T., Poor, C. B., Owens, C. P., Balderas, M. A., Fabian, M., Olson, J. S., Murphy, F., Balkabasi, E., Honsa, E. S., He, C., Goulding, C. W., and Maresso, A. W. (2012) Differential function of Lip residues in the mechanism and biology of an anthrax hemophore, *PLoS Pathog.* 8.
- [24] Liu, M., Su, J. G., Kong, R., Sun, T. G., Tan, J. J., Chen, W. Z., and Wang, C. X. (2008) Molecular dynamics simulations of the bacterial periplasmic heme binding proteins ShuT and PhuT, *Biophys. Chem.* 138, 42-49.
- [25] Poole, K., and Braun, V. (1988) Iron regulation of *Serratia marcescens* hemolysin gene expression, *Infect. Immun* 56, 2967-2971.
- [26] Angerer, A., Klupp, B., and Braun, V. (1992) Iron transport systems of *Serratia marcescens*, *J. Bacteriol* 174, 1378-1387.
- [27] Létoffé, S., Ghigo, J. M., and Wandersman, C. (1994) Secretion of the *Serratia marcescens* HasA protein by an ABC transporter, *J. Bacteriol* 176, 5372-5377.
- [28] Létoffé, S., Ghigo, J. M., and Wandersman, C. (1994) Secretion of the *Serratia marcescens* HasA protein by an ABC transporter, *Journal of Bacteriology.* 176, 5372-5377.
- [29] Létoffé, S., Ghigo, J. M., and Wandersman, C. (1994) Iron acquisition from heme and hemoglobin by a *Serratia marcescens* extracellular protein, *Proc. Natl. Acad. Sci. USA* 91, 9876-9880.
- [30] Arnoux, P., Haser, R., Izadi, N., Lecroisey, A., Delepierre, M., Wandersman, C., and Czjzek, M. (1999) The crystal structure of HasA, a hemophore secreted by *Serratia marcescens*, *Nat. Struct. Biol.* 6, 516-520.

- [31] Zubieta, C., Krishna, S. S., Kapoor, M., Kozbial, P., McMullan, D., Axelrod, H. L., Miller, M. D., Abdubek, P., Ambing, E., Astakhova, T., Carlton, D., Chiu, H. J., Clayton, T., Deller, M. C., Duan, L., Elsliger, M. A., Feuerhelm, J., Grzechnik, S. K., Hale, J., Hampton, E., Han, G. W., Jaroszewski, L., Jin, K. K., Mock, H. E., Knuth, M. W., Kumar, A., Marciano, D., Morse, A. T., Nigoghossian, E., Mach, L., Oommachen, S., Reyes, R., Rife, C. L., Schimmel, P., van den Bedem, H., Weekes, D., White, A., Xu, Q. P., Hodgson, K. O., Wooley, J., Deacon, A. M., Godzik, A., Lesley, S. A., and Wilson, I. A. (2007) Crystal structures of two novel dye-decolorizing peroxidases reveal a beta-bar fold with a conserved heme-binding motif, *Proteins-Structure Function and Bioinformatics* 69, 223-233.
- [32] Eakanunkul, S., Lukat-Rodgers, G. S., Sumithran, S., Ghosh, A., Rodgers, K. R., Dawson, J. H., and Wilks, A. (2005) Characterization of the periplasmic heme-binding protein ShuT from the heme uptake system of *Shigella dysenteriae*, *Biochemistry* 44, 13179-13191.
- [33] Wilks, A., and Ikeda-Saito, M. (2014) Heme utilization by pathogenic bacteria: Not all pathways lead to biliverdin, *Acc. Chem. Res.* 47, 2291-2298.
- [34] Benson, D. R., and Rivera, M. (2013) Heme uptake and metabolism in bacteria, *Met. Ions Life Sci* 12, 279-332.
- [35] Nobles, C. L., and Maresso, A. W. (2011) The theft of host heme by Gram-positive pathogenic bacteria, *Metallomics* 3, 788-796.
- [36] Zhou, H. X. (1997) Control of reduction potential by protein matrix - lesson from a spherical protein model, *J. Biol. Inorganic Chemistry* 2, 109-113.
- [37] Wilson, G. S. (1978) Determination of oxidation-reduction potentials, *Methods Enzymol.* 54, 396-410.
- [38] Tezcan, F. A., Winkler, J. R., and Gray, H. B. (1998) Effects of ligation and folding on reduction potentials of heme proteins, *J. Am. Chem. Soc.* 120, 13383-13388.
- [39] Mattle, D., Zeltina, A., Woo, J. S., Goetz, B. A., and Locher, K. P. (2010) Two stacked heme molecules in the binding pocket of the periplasmic heme-binding protein HmuT from *Yersinia pestis*, *J. Mol. Biol.* 404, 220-231.
- [40] Muraki, N., and Aono, S. (2015) Structural basis for heme recognition by HmuT responsible for heme transport to the heme transporter in *Corynebacterium glutamicum*, *Chem. Lett.* 45, 24-26.
- [41] Draganova, E. B., Adrian, S. A., Lukat-Rodgers, G. S., Keutcha, C. S., Schmitt, M. P., Rodgers, K. R., and Dixon, D. W. (2016) *Corynebacterium diphtheriae* HmuT: Dissecting the roles of conserved residues in heme pocket stabilization, *J. Biol. Inorg. Chem.* 21, 875-886.
- [42] Oldham, M. L., Brash, A. R., and Newcomer, M. E. (2005) The structure of coral allene oxide synthase reveals a catalase adapted for metabolism of a fatty acid hydroperoxide, *Proc. Natl. Acad. Sci. U. S. A.* 102, 297-302.
- [43] Fita, I., and Rossmann, M. G. (1985) The active center of catalase, *J. Mol. Biol.* 185, 21-37.
- [44] Pakhomova, S., Gao, B., Boeglin, W. E., Brash, A. R., and Newcomer, M. E. (2009) The structure and peroxidase activity of a 33-kDa catalase-related protein from *Mycobacterium avium* ssp. paratuberculosis, *Protein Sci* 18, 2559-2568.
- [45] Muraki, N., Kitatsuji, C., Ogura, M., Uchida, T., Ishimori, K., and Aono, S. (2016) Structural characterization of heme environmental mutants of CgHmuT that shuttles heme molecules to heme transporters, *Int. J. Mol. Sci.* 17.

- [46] Lei, B., Smoot, L. M., Menning, H. M., Voyich, J. M., Kala, S. V., Deleo, F. R., Reid, S. D., and Musser, J. M. (2002) Identification and characterization of a novel heme-associated cell surface protein made by *Streptococcus pyogenes*, *Infection and Immunity* 70, 4494-4500.
- [47] Zhu, H., Liu, M. Y., and Lei, B. F. (2008) The surface protein Shr of *Streptococcus pyogenes* binds heme and transfers it to the streptococcal heme-binding protein Shp, *BMC Microbiol.* 8, 15.
- [48] Sachla, A. J., Le Breton, Y., Akhter, F., Mciver, K. S., and Eichenbaum, Z. (2014) The crimson conundrum: Heme toxicity and tolerance in GAS, *Front. Cell. Infect. Microbiol.* 4.
- [49] Ouattara, M., Cunha, E. B., Li, X., Huang, Y. S., Dixon, D. W., and Eichenbaum, Z. (2010) Shr of Group A streptococcus is a new type of composite NEAT protein involved in sequestering haem from methaemoglobin, *Mol. Microbiol.* 78, 739-756.
- [50] Lei, B. F., Liu, M. Y., Prater, C. I., Kala, S. V., Deleo, F. R., and Musser, J. M. (2003) Identification and characterization of HtsA, a second heme-binding protein made by *Streptococcus pyogenes*, *Infect. Immun.* 71, 5962-5969.
- [51] Andrade, M. A., Ciccarelli, F. D., Perez-Iratxeta, C., and Bork, P. (2002) NEAT: A domain duplicated in genes near the components of a putative Fe(3+) siderophore transporter from Gram-positive pathogenic bacteria, *Genome Biol.* 3, RESEARCH0047.
- [52] Honsa, E. S., Maresso, A. W., and Highlander, S. K. (2014) Molecular and evolutionary analysis of NEAr-iron Transporter (NEAT) domains, *PLoS One* 9.
- [53] Gaudin, C. F. M., Grigg, J. C., Arrieta, A. L., and Murphy, M. E. P. (2011) Unique heme-iron coordination by the hemoglobin receptor IsdB of *Staphylococcus aureus*, *Biochemistry* 50, 5443-5452.
- [54] Plum, M., Muryoi, N., Heinrichs, D. E., and Stillman, M. J. (2008) Heme binding in the NEAT domains of IsdA and IsdC of *Staphylococcus aureus*, *J. Inorg. Biochem.* 102, 480-488.
- [55] Balderas, M. A., Nobles, C. L., Honsa, E. S., Alicki, E. R., and Maresso, A. W. (2012) Hal is a *Bacillus anthracis* heme acquisition protein, *J. Bacteriol.* 194, 5513-5521.
- [56] Malmirchegini, G. R., Sjodt, M., Shnitkind, S., Sawaya, M. R., Rosinski, J., Newton, S. M., Klebba, P. E., and Clubb, R. T. (2014) Novel mechanism of heme capture by Hbp2, the hemoglobin-binding hemophore from *Listeria monocytogenes*, *J. Biol. Chem.* 289, 34886-34899.
- [57] Ferrer, J. C., Guillemette, J. G., Bogumil, R., Inglis, S. C., Smith, M., and Mauk, A. G. (1993) Identification of Lys79 as an iron ligand in one form of alkaline yeast iso-1-ferricytochrome *c*, *J. Am. Chem. Soc.* 115, 7507-7508.
- [58] Cheesman, M. R., Thomson, A. J., Greenwood, C., Moore, G. R., and Kadir, F. (1990) Bis-methionine axial ligation of haem in bacterioferritin from *Pseudomonas aeruginosa*, *Nature* 346, 771-773.
- [59] Cheesman, M. R., Kadir, F. H. A., Albasseet, J., Almassad, F., Farrar, J., Greenwood, C., Thomson, A. J., and Moore, G. R. (1992) EPR and magnetic circular-dichroism spectroscopic characterization of bacterioferritin from *Pseudomonas aeruginosa* and *Azotobacter vinelandii*, *Biochem. J.* 286, 361-367.
- [60] Cheesman, M. R., Lebrun, N. E., Kadir, F. H. A., Thomson, A. J., Moore, G. R., Andrews, S. C., Guest, J. R., Harrison, P. M., Smith, J. M. A., and Yewdall, S. J. (1993) Heme and

- nonheme iron sites in *Escherichia coli* bacterioferritin - spectroscopic and model-building studies, *Biochem. J.* 292, 47-56.
- [61] George, G. N., Richards, T., Bare, R. E., Gea, Y., Prince, R. C., Stiefel, E. I., and Watt, G. D. (1993) Direct observation of bis-sulfur ligation to the heme of bacterioferritin, *J. Am. Chem. Soc.* 115, 7716-7718.
- [62] Wiederkehr, R. S., Hoops, G. C., Aslan, M. M., Byard, C. L., and Mendes, S. B. (2009) Investigations on the Q and CT Bands of Cytochrome c Submonolayer Adsorbed on an Alumina Surface Using Broadband Spectroscopy with Single-Mode Integrated Optical Waveguides, *Journal of Physical Chemistry C* 113, 8306-8312.
- [63] Tiedemann, M. T., and Stillman, M. J. (2012) Heme binding to the IsdE(M78A; H229A) double mutant: Challenging unidirectional heme transfer in the iron-regulated surface determinant protein heme transfer pathway of *Staphylococcus aureus*, *J. Biol. Inorg. Chem.* 17, 995-1007.
- [64] Ran, Y. C., Liu, M. Y., Zhu, H., Nygaard, T. K., Brown, D. E., Fabian, M., Dooley, D. M., and Lei, B. F. (2010) Spectroscopic identification of heme axial ligands in HtsA that are involved in heme acquisition by *Streptococcus pyogenes*, *Biochemistry* 49, 2834-2842.
- [65] Ran, Y. C., Zhu, H., Liu, M. Y., Fabian, M., Olson, J. S., Aranda, R. I., Phillips, G. N., Dooley, D. M., and Lei, B. (2007) Bis-methionine ligation to heme iron in the streptococcal cell surface protein Shp facilitates rapid hemin transfer to HtsA of the HtsABC transporter, *J. Biol. Chem.* 282, 31380-31388.
- [66] Barker, P. D., Nerou, E. P., Cheesman, M. R., Thomson, A. J., de Oliveira, P., and Hill, H. A. (1996) Bis-methionine ligation to heme iron in mutants of cytochrome b₅₆₂. 1. Spectroscopic and electrochemical characterization of the electronic properties, *Biochemistry* 35, 13618-13626.
- [67] Zhong, L. H., Wen, X., Rabinowitz, T. M., Russell, B. S., Karan, E. F., and Bren, K. L. (2004) Heme axial methionine fluxionality in *Hydrogenobacter thermophilus* cytochrome c552, *Proc. Natl. Acad. Sci. USA* 101, 8637-8642.
- [68] Wen, X., Patel, K. M., Russell, B. S., and Bren, K. L. (2007) Effects of heme pocket structure and mobility on cytochrome c stability, *Biochemistry* 46, 2537-2544.
- [69] Du, J., Sono, M., and Dawson, J. H. (2011) Ferric His93Gly myoglobin cavity mutant and its complexes with thioether and selenolate as heme protein models, *J. Porph. Phthalo.* 15, 29-38.
- [70] Lauth de Almeida Torres, R. S., de Almeida Torres, R. P., Smeesters, P. R., Palmeiro, J. K., de Messias-Reason, I. J., and Dalla-Costa, L. M. (2011) Group A Streptococcus antibiotic resistance in Southern Brazil: A 17-Year surveillance study, *Microbial Drug Resistance* 17, 313-319.
- [71] Willems, R. J. L., Hanage, W. P., Bessen, D. E., and Feil, E. J. (2011) Population biology of Gram-positive pathogens: High-risk clones for dissemination of antibiotic resistance, *FEMS Microbiol. Rev.* 35, 872-900.
- [72] Pires, R., Ardanuy, C., Rolo, D., Morais, A., Brito-Avo, A., Goncalo-Marques, J., Linares, J., and Santos-Sanches, I. (2010) Emergence of ciprofloxacin-nonsusceptible *Streptococcus pyogenes* isolates from healthy children and pediatric patients in Portugal, *Antimicrob. Agents Chemother.* 54, 2677-2680.
- [73] Rodgers, K. R., and Lukat-Rodgers, G. S. (2014) Biophysical perspectives on the acquisition, transport, and trafficking of heme in bacteria, In *Handbook of Porphyrin Science with Applications to Chemistry, Physics, Materials Science, Engineering,*

- Biology and Medicine, Vol. 30: Heme Proteins, Part II* (Ferreira, G. C., Kadish, K. M., Smith, K. M., and Guillard, R., Eds.), pp 251-309, World Scientific, Hackensack, N.J.
- [74] Fernández, A., Lechardeur, D., Derre-Bobillot, A., Couve, E., Gaudu, P., and Gruss, A. (2010) Two coregulated efflux transporters modulate intracellular heme and protoporphyrin IX availability in *Streptococcus agalactiae*, *PLoS Pathog.* 6.
- [75] Kumarevel, T. (2012) The MarR family of transcriptional regulators - A structural perspective, In *Antibiotic Resistant Bacteria - A Continuous Challenge in the New Millennium* (Pana, M., Ed.), pp 403-418, InTech.
- [76] Owens, C. P., Du, J., Dawson, J. H., and Goulding, C. W. (2012) Characterization of heme ligation properties of Rv0203, a secreted heme binding protein involved in *Mycobacterium tuberculosis* heme uptake, *Biochemistry* 51, 1518-1531.
- [77] Tullius, M. V., Harmston, C. A., Owens, C. P., Chim, N., Morse, R. P., McMath, L. M., Iniguez, A., Kimmey, J. M., Sawaya, M. R., Whitelegge, J. P., Horwitz, M. A., and Goulding, C. W. (2011) Discovery and characterization of a unique mycobacterial heme acquisition system, *Proc. Natl. Acad. Sci. U. S. A.* 108, 5051-5056.
- [78] Bommer, J. C., and Hambricht, P. (2002) General methods for tetrapyrroles, In *Heme, Chlorophyll, and Bilins. Methods and Protocols* (Smith, A. G., and Witty, M., Eds.) 1 ed., pp 39-68, Humana Press, Totowa, NJ.
- [79] Radhakrishnan, A., Kumar, N., Wright, C. C., Chou, T. H., Tringides, M. L., Bolla, J. R., Lei, H. T., Rajashankar, K. R., Su, C. C., Purdy, G. E., and Yu, E. W. (2014) Crystal structure of the transcriptional regulator Rv0678 of *Mycobacterium tuberculosis*, *J. Biol. Chem.* 289, 16526-16540.
- [80] Hao, Z. Y., Lou, H. B., Zhu, R. F., Zhu, J. H., Zhang, D. M., Zhao, B. X. S., Zeng, S. Z., Chen, X., Chan, J., He, C., and Chen, P. R. (2014) The multiple antibiotic resistance regulator MarR is a copper sensor in *Escherichia coli*, *Nat. Chem. Biol.* 10, 21-U48.
- [81] Davis, J. R., Brown, B. L., Page, R., and Sello, J. K. (2013) Study of PcaV from *Streptomyces coelicolor* yields new insights into ligand-responsive MarR family transcription factors, *Nucleic Acids Res.* 41, 3888-3900.
- [82] Reedy, C. J., Elvekrog, M. M., and Gibney, B. R. (2008) Development of a heme protein structure-electrochemical function database, *Nucleic Acids Res.* 36, D307-D313.
- [83] Birukou, I., Seo, S. M., Schindler, B. D., Kaatz, G. W., and Brennan, R. G. (2014) Structural mechanism of transcription regulation of the *Staphylococcus aureus* multidrug efflux operon mepRA by the MarR family repressor MepR, *Nucleic Acids Res.* 42, 2774-2788.
- [84] Yang, J. Y., Yan, R. X., Roy, A., Xu, D., Poisson, J., and Zhang, Y. (2015) The I-TASSER Suite: Protein structure and function prediction, *Nature Methods* 12, 7-8.
- [85] Gasteiger, E., Hoogland, C., Gattiker, A., Duvaud, S., Wilkins, M. R., Appel, R. D., and Bairoch, A. (2005) Protein identification and analysis tools on the ExPASy server, In *The Proteomics Protocols Handbook* (Walker, J. M., Ed.), pp 571-607, Humana Press, Totowa, N.J.
- [86] Muraki, N., Kitatsuji, C., and Aono, S. (2015) A new biological function of heme as a signaling molecule, *J. Porph. Phthalo.* 19, 9-20.
- [87] Hira, S., Tomita, T., Matsui, T., Igarashi, K., and Ikeda-Saito, M. (2007) Bach1, a heme-dependent transcription factor, reveals presence of multiple heme binding sites with distinct coordination structure, *IUBMB Life* 59, 542-551.

- [88] Du, J., Sono, M., and Dawson, J. H. (2011) The H93G myoglobin cavity mutant as a versatile scaffold for modeling heme iron coordination structures in protein active sites and their characterization with magnetic circular dichroism spectroscopy, *Coord. Chem. Rev.* 255, 700-716.
- [89] Sachla, A. J., and Eichenbaum, Z. (2016) The GAS PefCD exporter is a MDR system that confers resistance to heme and structurally diverse compounds, *BMC Microbiol.* 16.
- [90] Lechardeur, D., Cesselin, B., Liebl, U., Vos, M. H., Fernandez, A., Brun, C., Gruss, A., and Gaudu, P. (2012) Discovery of Intracellular Heme-binding Protein HrtR, Which Controls Heme Efflux by the Conserved HrtB-HrtA Transporter in *Lactococcus lactis*, *J. Biol. Chem.* 287, 4752-4758.